Mangrove Monitoring Using Airborne VNIR in the Espiritu Santo Bay Area, Central Texas Coast

Rebecca Brown, Jeffrey G. Paine, Kutalmis Saylam,
Thomas A. Tremblay, John R. Andrews, and Aaron Averett

Final Report

September 2016

QAe5073

Page intentionally blank

MANGROVE MONITORING USING AIRBORNE VNIR
IN THE ESPIRITU SANTO BAY AREA, CENTRAL TEXAS COAST

by

Rebecca Brown, Jeffrey G. Paine, Kutalmis Saylam, Thomas A. Tremblay,
John R. Andrews, and Aaron Averett

Bureau of Economic Geology
John A. and Katherine G. Jackson School of Geosciences
The University of Texas at Austin
University Station, Box X
Austin, Texas 78713

Corresponding author
jeff.paine@beg.utexas.edu
(512) 471-1260
TBPG License No. 3776

Page intentionally blank

CONTENTS

FIGURES

TABLES

Page intentionally blank

SUMMARY

We conducted a pilot airborne hyperspectral survey of the Espiritu Santo Bay area on the central Texas coast in November 2015 to examine whether imagery from visible and near-infrared (VNIR) wavelengths could be used to rapidly and accurately map black mangrove (*Avicennia germinans*) habitat. The airborne insrument is a pushbroom (scanline) hyperspectral sensor having 399 spectral bands between 400 and 1,000 nanometers (nm) wavelength. Ground-based spectra of black mangrove, smooth cordgrass (*Spartina alterniflora*), calibration targets (black, white, and gray), and open bay water were acquired during the airborne survey along southwestern and northeastern Espiritu Santo Bay. VNIR data from the airborne survey were directly georeferenced using GPS and inertial navigation system (INS) data. This approach adequately removed waviness and spatial distortion in the imagery, but produced a loose georeferencing accuracy of only a few tens of meters or better. Higher quality GPS and INS data would be required to improve the direct georeferencing accuracy. To identify mangrove habitat, we classified airborne VNIR imagery having a Normalized Difference Vegetation Index (NDVI) greater than 0.2 as vegetation, then discriminated mangrove from non-mangrove habitat using intensity differences at 550 nm wavelength. Classification checks at 75 sites yielded an overall accuracy of 75 percent when using manual mapping based on 2013 color infrared imagery and airborne lidar-derived topographic data as ground truth. Of the mangrove sites checked, 85 percent were classified accurately using the VNIR-based approach. Most areas misclassified as mangrove were readily identified by comparison with mangrove expression on color infrared imagery and topographic data and were removed from the areas classified as mangrove. Analysis of the 2015 airborne VNIR data yielded 1,499 hectares (ha) classified as mangrove, which is about 20 percent higher than mangrove area (1,199 ha) determined using manual methods based on 2013 data. Both approaches indicate mangrove extent has expanded from its area documented in inventories based on 1979 and 2001 aerial photographs and is similar to a 1500 ha habitat estimate from the mid-1970s. Current mangrove extent suggests that mangrove habitat has recovered from significant areal reductions attributed to two severe and prolonged freezes in 1983 and 1989.

Page intentionally blank

INTRODUCTION

Black mangrove (*Avicennia germinans*, Fig. 1) is an increasingly abundant component of salt marshes along the Texas Coastal Bend. Mangroves and other wetland habitat on the Texas coast can be manually mapped from aerial photographs with supporting field studies (e.g. Sherrod, and McMillan, 1981; Shew and others, 1981; U.S. Fish and Wildlife Service, 1983; White and others, 2002), but availability of advanced airborne instruments such as lidar and hyperspectral cameras has presented an opportunity to evaluate how these instruments might be used to facilitate the detection of coastal habitat in general and mangroves in particular.

We conducted an airborne hyperspectral survey of Espiritu Santo Bay and Matagorda Island in Calhoun County, Texas to test whether hyperspectral imagery can be used to map the extent of black mangrove in Texas' Coastal Bend area. Recent studies indicate that mangrove distribution in Texas is increasing, and is a contributing factor in salt marsh loss (Armitage and others,

Figure 1. Black mangrove along the Espiritu Santo Bay shoreline, November 18, 2015. Photograph was taken by T. Tremblay during the airborne hyperspectral survey.

1

2015). Mangroves can replace smooth cordgrass (*Spartina alterniflora*) in salt marsh, which is the preferred habitat of the blue crab, a significant food source for the endangered whooping crane (*Grus americana*). Increases in winter temperatures associated with climate change (Guo and others, 2013) may accelerate the mangrove expansion because the species is cold-sensitive, and periodic freezes in the Texas' Gulf coast waters typically limit their growth and northward spread. To address these concerns, there is a need for timely and accurate mangrove mapping on the Texas coast and in other coastal regions where mangrove is spreading.

The Espiritu Santo Bay survey (Fig. 2), flown in November 2015, was the first airborne hyperspectral survey completed using the Bureau's visible and near-infrared (VNIR) spectral camera. Ancillary goals for this initial airborne VNIR survey included evaluating and improving data acquisition, calibration, and processing procedures for the VNIR camera.

The VNIR camera contains a sensor that allows for fine spectral resolution by measuring the electromagnetic energy across hundreds of narrow wavelength ranges that can be used to identify the unique signatures reflected from objects (Fig. 3). The VNIR camera used in this survey is a pco.edge 5.5 model manufactured by PCO Tech (Fig. 4a) and modified by Opto-Knowledge Systems, Inc. The camera has a scientific CMOS (sCMOS) sensor that is capable of detecting signals at wavelengths between 400 and 1,000 nanometers (nm), covering the VNIR region of the electromagnetic spectrum (Table 1). Introduced in 2009, sCMOS was designed to overcome the deficiencies of previous CMOS and CCD sensors such as limited dynamic range and sensitivity (Coates and others, 2009).

The VNIR camera includes a convex diffraction grating that splits incoming light into narrow wavelength ranges, resulting in monochromatic light dispersed across the sensor (Fig. 4b). This allows distinct spectral wavelengths to be mapped on the sensor and recorded as a hyperspectral image (Dell'Endice and others, 2009). Hyperspectral data files can be considered a three-dimensional "cube" that includes the two lateral spatial dimensions (Fig. 5). The third dimension is

2
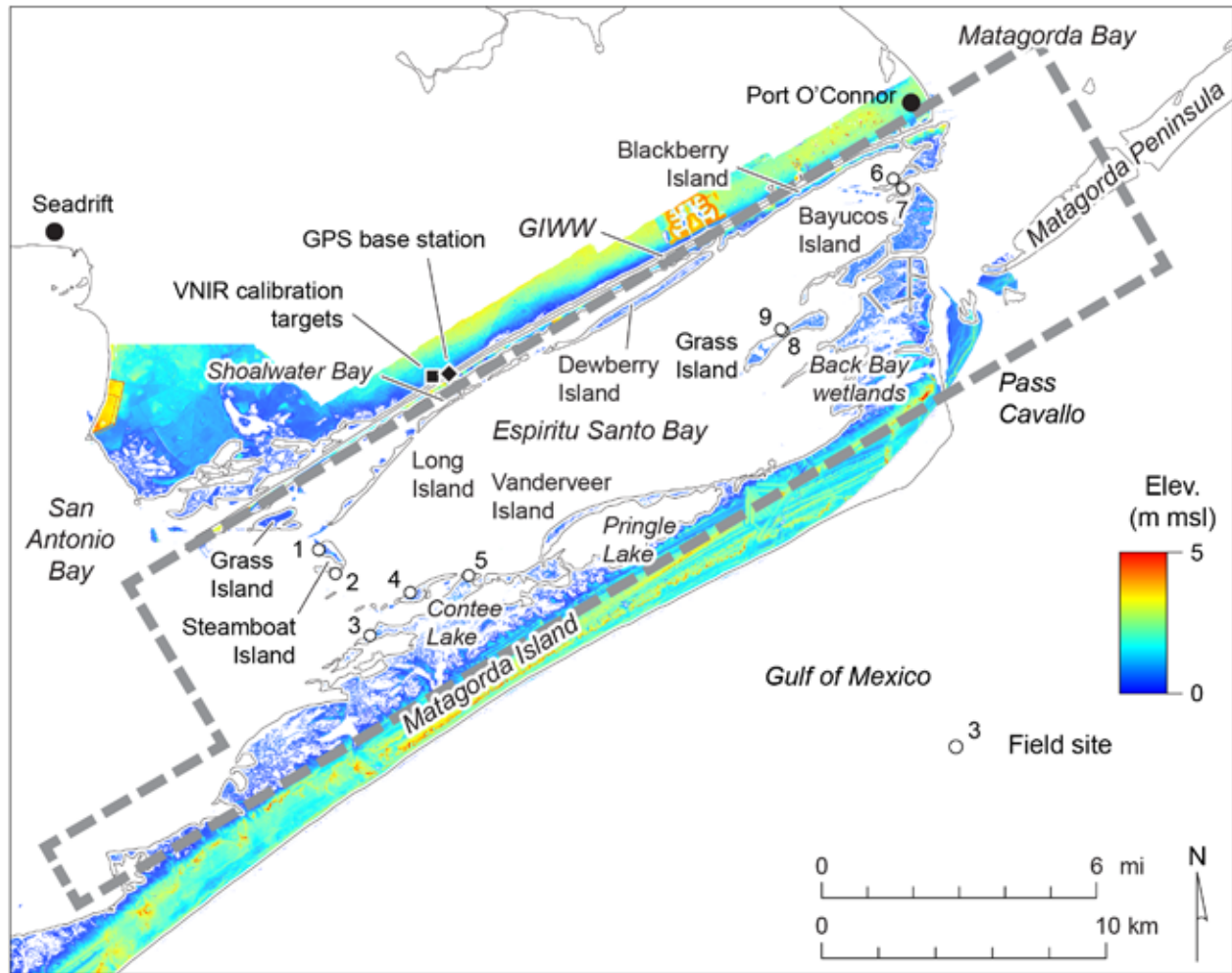
Figure 2. Map of the Espiritu Santo Bay study area showing the outline of the November 2015 airborne VNIR survey, field sites visited during the airborne survey, and the location of VNIR calibration targets and a GPS base station. These locations are superimposed on a digital elevation model (DEM) constructed from data acquired during an airborne lidar survey of the bay in June 2013.

the spectrum for each pixel. A data capture software application written at the Bureau employs a line-by-line read out ("pushbroom") design for this sensor.

MANGROVE REMOTE SENSING

Mangroves are woody shrubs or trees adapted to flooded, saline habitats; they flourish in inter-tidal zones in the tropics and subtropics (Spalding and others, 2010a). The black mangrove is the only mangrove species commonly found in Texas (Yang and others, 2009; Richardson and
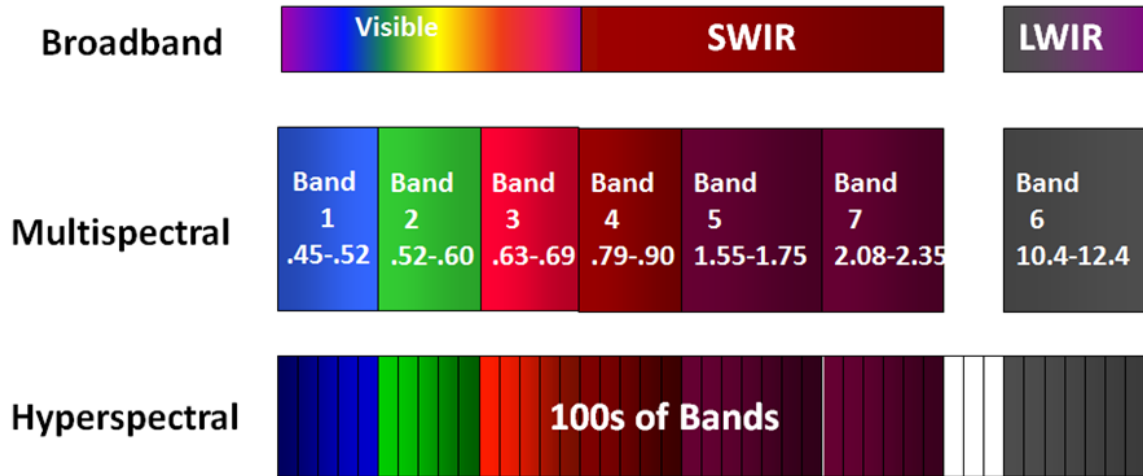
Figure 3. Comparison of multispectral and hyperspectral data (after Elowitz, undated).
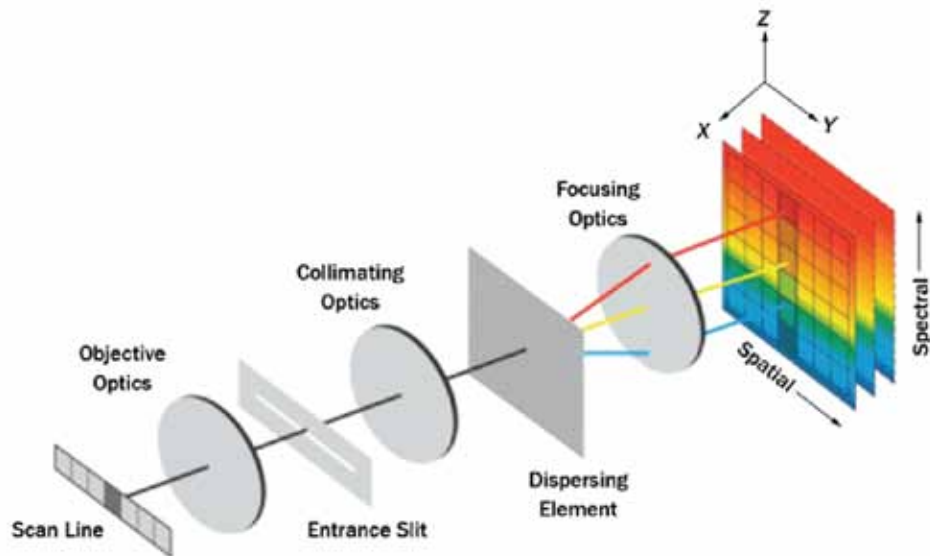
Figure 4. (a) pco.edge 5.5 VNIR camera and (b) pushbroom scanner component configuration.

Table 1. Modified pco.edge 5.5 spectral camera specifications.

Resolution (cross track x along track)	2,560 x 2,160
Pixel size	6.5 μm x 6.5 μm
Focal length	23 mm
Number of spectral channels	399
Spectral range	400 to 1,000 nm
Dynamic range	16 bits
Global shutter exposure	10 to 100 μs
Maximum frame rate	50 fps
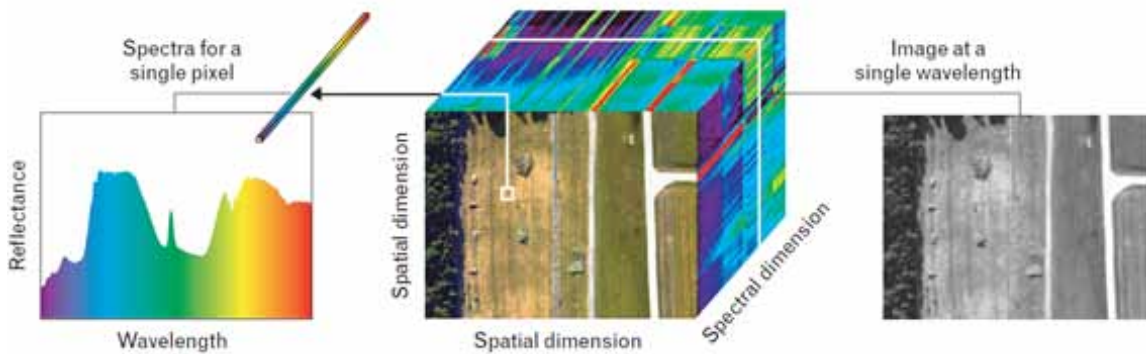
Figure 5. Hyperspectral data represented as a three-dimensional "cube."

King, 2011). According to Spalding and others (2010b), there are only dwarf or shrub communities of black mangroves in Texas because cool air temperatures in the northern and central Gulf of Mexico limit their growth. In these Gulf coast waters, mangroves do not form forests or dense communities, and may die off during colder years.

Mangroves, like all vegetation, have a distinct spectral response. Low reflectivity in the shorter, visible wavelengths is caused primarily by chlorophyll absorption. There is a steep increase in reflectance at wavelengths longer than 700 nm due to the strong scattering of light in the internal cell structure of leaves (Jensen, 2007; Klemas, 2015). This jump in reflectance at NIR wavelengths is called the "red edge" and can be used to identify vegetation cover and determine vegetation health (Fig. 6). While identifying vegetation cover is well understood, distinguishing

5
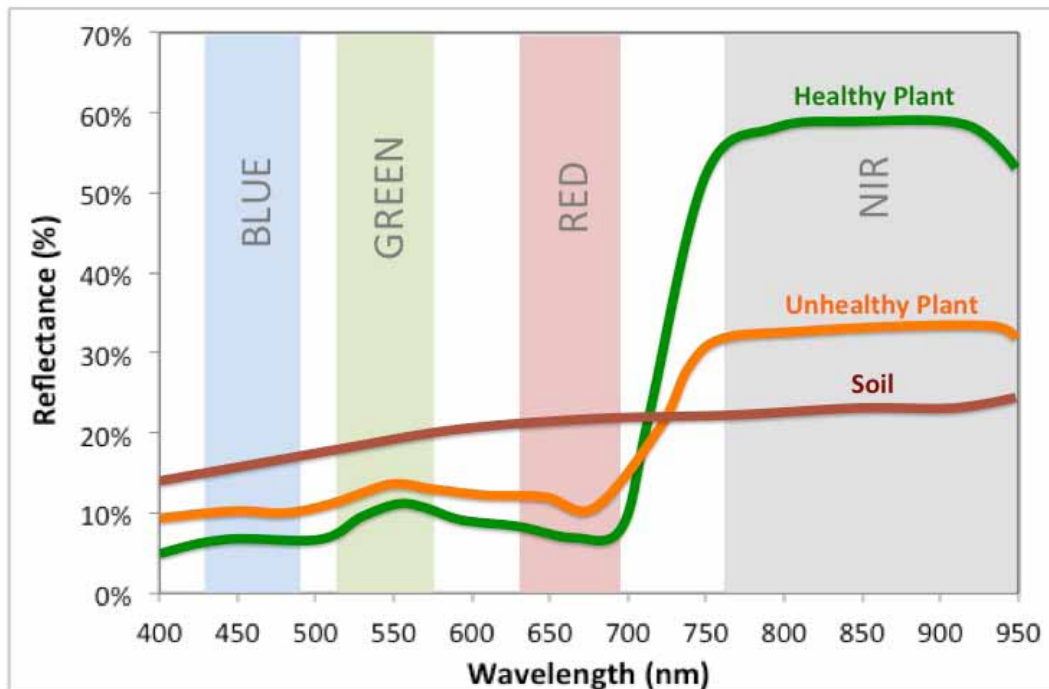
Figure 6. Typical expected reflection spectra of vegetation and soil.

individual vegetation species can be difficult because their similar physical composition results in highly correlated reflectance values (Adam and others, 2010). To discriminate imagery at the species level, narrow spectral bands must be chosen to identify unique features caused by species-specific properties, including chlorophyll content, leaf structure, and pigment concentration (Vaiphasa and others, 2005; Adam and others, 2010).

Applying remote sensing methods to mapping wetland plants, such as mangroves, is more challenging than detecting terrestrial plants for several reasons. The observed spectra of wetland species can vary significantly due to environmental factors. All remotely sensed data are affected by atmospheric properties, and the high humidity of coastal areas can contribute to the captured reflectance spectra (Blasco and others, 1998, 2005). The reflectance spectra of flooded wetland vegetation is also mixed with, and attenuated by, spectral contributions from underlying water and wet soil (Adam and others, 2010; Rundquist and others, 2001). Furthermore, wetlands are

6

dynamic systems with many variables that can affect radiometric properties, such as salinity, daily tidal changes, and seasonal flooding (Blasco and others, 1998; Lang and McCarty, 2008). Achievable spatial resolution can also be a limiting factor in discriminating mangroves, because mangroves commonly grow in small, distinct patches (Klemas, 2015; Green and others, 1998). Researchers have concluded that a combination of high spatial and spectral resolution is needed to adequately map wetlands (Green and others, 1998; Lang and McCarty, 2008; Adam and others, 2010).

The earliest wetland surveys were completed with aerial photography and manual photo interpretation, and later satellites with multispectral sensors such as Landsat and SPOT became popular for mapping mangroves on larger scale (Blasco and others, 2005; Adam and others, 2010; Klemas, 2015). In some cases, mangrove spectra cannot be distinguished from other vegetation types because of the coarse spectral and spatial resolution of satellites.

Airborne hyperspectral cameras can overcome these limitations by providing high spatial resolution and narrow spectral band resolution required to identify species-specific features. Several studies have used laboratory spectral measurements to isolate wavelengths that best discriminate the mangroves (Vaiphasa and others, 2005; Wang and Sousa, 2009; Zhang and others, 2014). Their results, summarized in Table 2, suggest that sampling along the red-edge (690 to 730 nm) and further into the VNIR wavelength (700 to 2,000 nm) are key to differentiating mangroves spectrally. This observation is echoed by Adam and others (2010) whose literature review concluded that "most of the previous studies have stated that wetland vegetation have greatest variation in the near infrared and red-edge regions." Additionally, some field studies have used transforms such as the minimum noise fraction (MNF) to re-order hyperspectral data based on information content and reduce the hundreds of bands captured down to a dozen or so transformed bands (Hirano and others, 2003; Christian and Krishnayya, 2009; Yang and others, 2009).

Previous studies such as these were used as a base to understand and determine the unique spectral features of black mangroves on the Texas coast. Many airborne spectral surveys have

7

Table 2. Hyperspectral bands chosen for mangrove discrimination.

Study	Wavelengths (nm)
Vaiphasa and others (2005)	720, 1277, 141, 1644
Wang and Sousa (2009)	490, 500, 630, 770, 780, 790, 800
Zhang and others (2014)	520, 560, 650, 710, 760, 2100 and 2230

focused on differentiating mangrove species in the tropics where different species may grow in close proximity. There has been at least one hyperspectral study completed to identify the black mangrove on the Texas coastline (Yang and others, 2009).

METHODS

Field surveys conducted for this project included acquisition of hyperspectral imagery using an airborne platform and ground surveys using a field spectrometer to measure calibration target and vegetation spectra. Those spectra are included in the Appendix.

Airborne Data Acquisition

We acquired airborne hyperspectral data in the Espiritu Santo Bay area on November 18 and 19, 2015. The VNIR system was installed in a Cessna 206 operated by the Texas Department of Transportation (TxDOT) (Fig. 7) and flown from the Calhoun County Airport near Port Lavaca, Texas. The mission was flown at approximately 2,000 m altitude following a race-track pattern in which all flight lines were in the same flight direction (Fig. 8) and overlapped at least 40 percent. The image footprint on the ground for the cross-track scan line was about 1,450 m, translating to a cross-track resolution of about 0.6 m. The along-track, slit-based field of view was about 2.3 m.

Field Spectral Data Sampling

We conducted ground-truth field measurements in the Espiritu Santo Bay area using a portable spectrometer during the airborne VNIR survey. We visited nine sites by airboat on September 18, 2015 at Steamboat Island (sites 1 and 2, Fig. 2), along the bay shoreline of Matagorda Island (sites 3, 4, and 5), Bayucos Island (sites 6 and 7), and Grass Island (sites 8 and 9). At each site,

8

Figure 7. The Bureau's hyperspectral camera system installed in a Cessna 206.

several reflectance measurements (Appendix) were captured using an ASD FieldSpec 4 spectro-radiometer. We also acquired spectral signatures of black, gray, and white canvas targets deployed on the mainland adjacent to Shoalwater Bay (Fig. 2).

Geometric Correction and Georectification

Georeferencing and motion compensation of the airborne survey data were completed using a C# programming language application developed at the Bureau. The application integrates the time, position, and attitude information collected with the onboard GPS receiver and inertial navigation system (INS) to eliminate the roll, pitch, and attitude deformations of each data cube. The process was completed in three phases for each data cube.

In the initial phase, the precise position and orientation (heading) of the VNIR sensor at the time of each scanline was calculated by interpolating the measurements recorded by the INS. This
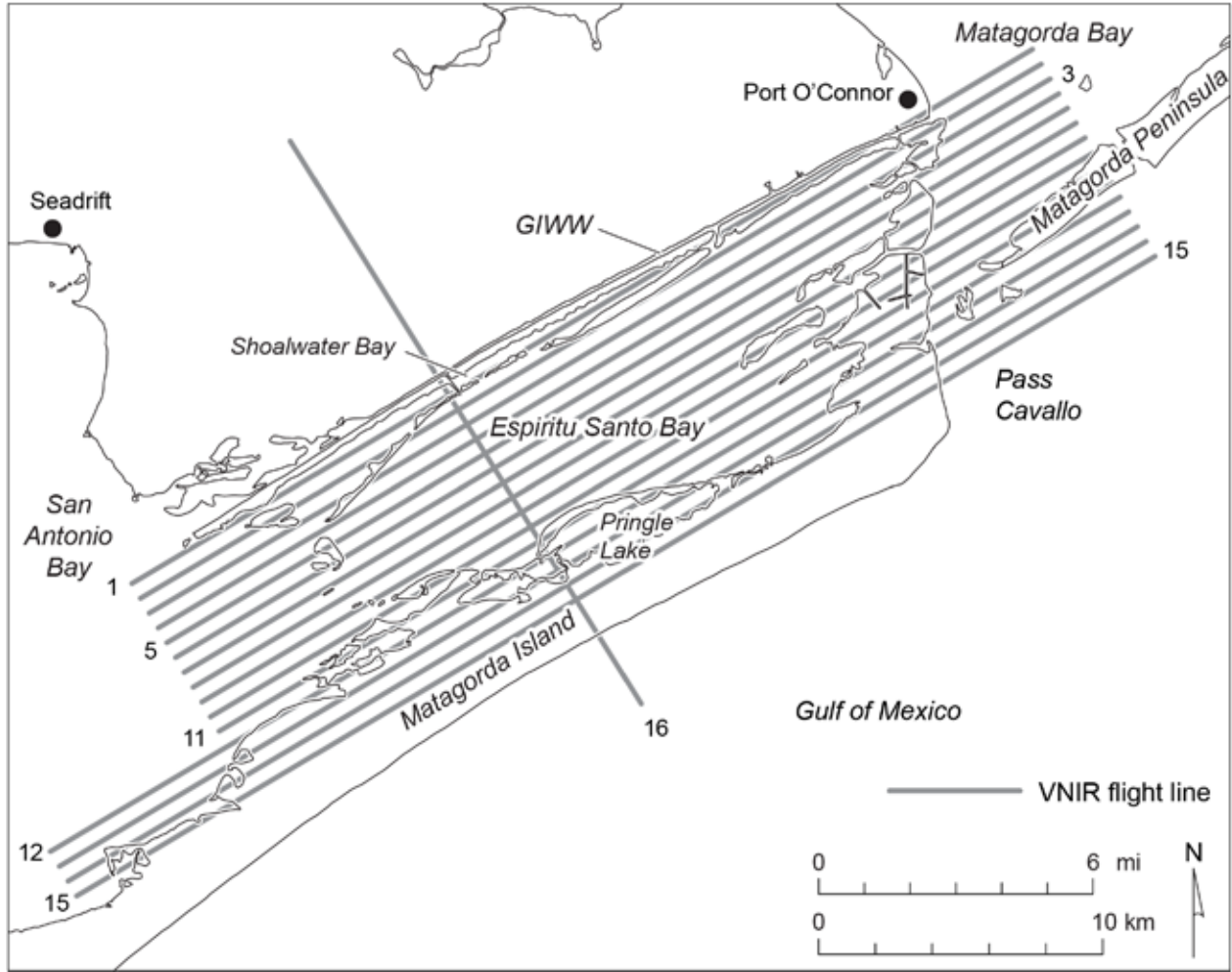
Figure 8. Airborne VNIR survey flight lines 1 through 16, November 18-19, 2015.

produced a data structure for each captured scanline that contains an x and y value in the WGS84 datum, elevation values relative to the geoid model (GEOID12B), and an interpolated roll, pitch, and attitude.

In the second phase, a set of coordinates in three-dimensional space representing the center of each pixel was projected to the ground. These values were calculated using the per-scanline position created in the first phase, the lens geometry of the camera, and an assumed elevation of the ground. The result of this process created a series of data structures for each pixel of each scanline, representing a projected location with x and y pixel values for each original pixel.

10

The final phase calculated the size of each data cube required to adjust for the motion of the camera, based on the minimum and maximum of x and y pixel values. The script iterates the set of data structures produced in phase two, fetches the originally observed band values from the raw data cube, and writes them into the appropriate pixels in the output cube.

After approximate georeferencing and motion compensation, each data cube was modified to have the required map projection using ENVI 5.3 image analysis software. ENVI creates a pseudo-spatial reference for these georeferenced cubes using four corner tie points. When displayed in ENVI, each pixel's latitude and longitude is derived from a map projection involving an affine transformation. Although ENVI can display spectral data on a generic map and analyze the data, tasks such as image mosaicking require the data cubes to have a map projection. Mosaicking a scene is necessary for data classification. For this study, a loosely georeferenced flight-line mosaic was created with each segment file projected to a standard spatial reference using ENVI's Reproject Raster task. We used 1-m resolution National Agricultural Imagery Program aerial imagery acquired in 2014 to align VNIR data to the NAD83 UTM Zone 14N datum.

Mosaicking an entire airborne mission created a very large output file (up to 7 GB) using just the red, green, blue bands. This is too large to cache in system memory to display or process. Instead, we mosaicked each band of the flight line separately using ENVI's Seamless Mosaic tool. After mosaicking each band, data values were scaled to between 0 and 255 and converted to a byte array which was composited to form an RGB image. Stitched and georeferenced RGB imagery is included as one of the project deliverables.

Radiometric Correction

Radiometric calibration establishes a relationship between the raw digital numbers collected by the system, which have no physical unit, and the quantitative measurements of reflectance. For satellite and airborne data, this is complicated by atmospheric effects, which greatly alter the signal reaching the camera sensor and create a complex relationship between at-sensor radiance and

surface reflectance values (Aspinall and others, 2002; Schowengerdt, 2007). Rigorous calibration methods involving complex atmospheric and radiative transfer models can correct atmospheric errors with a high degree of accuracy (Smith and Milton, 1999; Schowengerdt, 2007), but were beyond the scope of this initial study. Alternatively, a simplified calibration technique called the empirical line method (ELM) can be used to establish a relationship between at-sensor radiance and surface reflectance. This method creates a predictive equation to convert pixel values to reflectance based on the relationship between recorded sensor values and field measurements of the absolute reflectance of in-scene calibration targets (Staben and others, 2012). Acceptable results can be obtained using the empirical line fit if the calibration targets chosen sufficiently cover the range of sensor values (Smith and Milton, 1999).

For our survey, three 4.5 x 4.5 m tarpaulins in white, gray, and black canvas were prepared as in-scene targets and placed on the ground along Shoalwater Bay (Fig. 2). These targets were intended to represent a range of reflectance values, but were somewhat similar spectrally between wavelengths of about 750 to 1,000 nm (Fig. 9). To accurately calculate a correction value for each wavelength, ELM requires reference targets to have a range of intensity values at each wavelength, particularly light and dark points. This means that bands between 750 and 1,000 nm must either be excluded from calibration purposes, or only a single target should be used to calibrate the imagery. Use of a single target reduces the accuracy of the spectral correction and calibration.

We tested ELM using ENVI 5.3's Radiometric Correction toolbox, excluding wavelengths with insufficient intensity range (750 to 1,000 nm) for correction purposes. In the raw hyperspectral data, the calibration targets covered four or five spectrally pure pixels (Fig. 10). The average pixel value of all three targets was used as an input to ELM, along with the reflectance values of each target. Results using ELM were poor because an accurate predictive equation could not be established. The calibration targets had pixel values higher than those of vegetation, yielding negative reflectance values. Uncorrected pixel values were used for preliminary analysis.
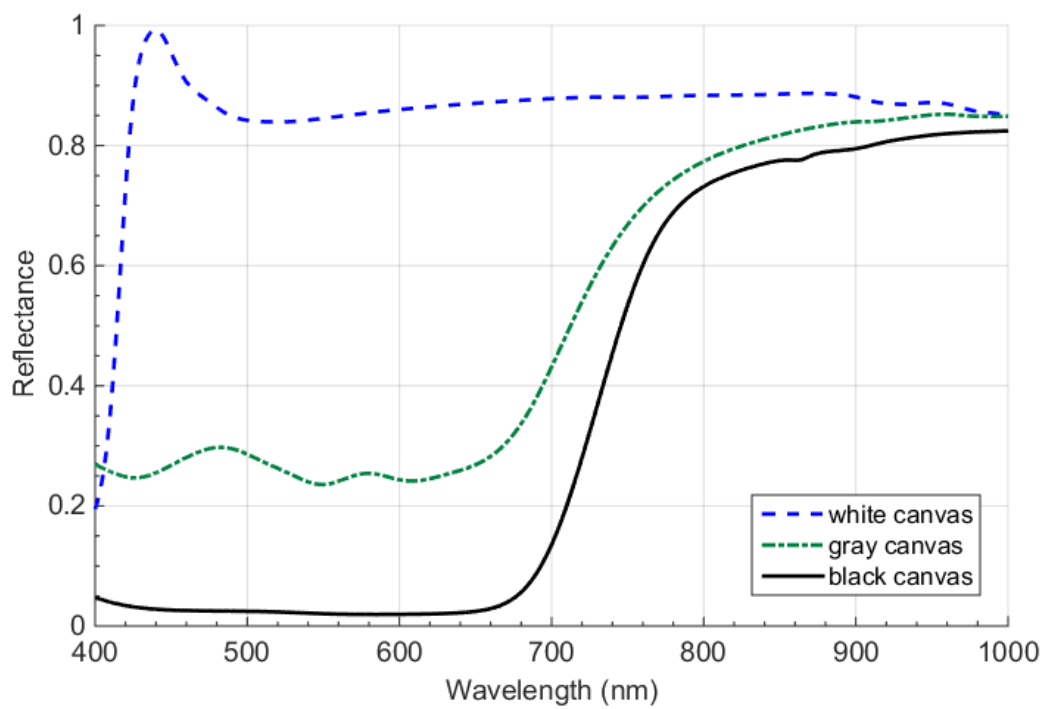
Figure 9. Reflectance curves of ground-based calibration targets.
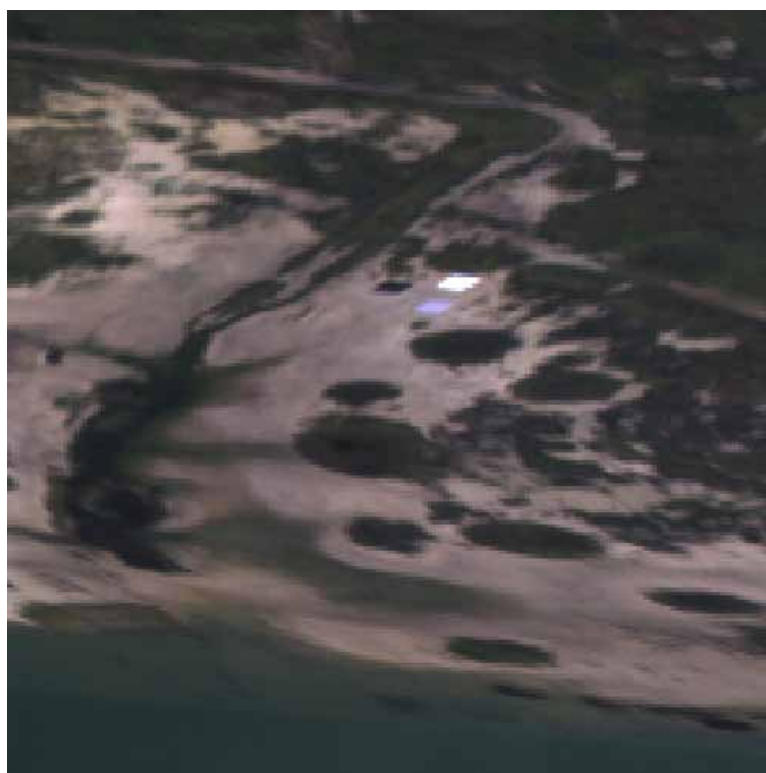
Figure 10. White, gray, and black tarp calibration targets captured by the VNIR sensor.

We constructed a mosaic of 16 lines of VNIR imagery (Fig. 11) that was loosely georeferenced using GPS and inertial navigation system (INS) data acquired during the airborne VNIR survey. This mosaic shows only three wavelength channels of the 399 acquired by the camera between 400 and 1,000 nm (Table 1). Owing to limitations of the GPS and INS employed for this survey, positional accuracy of the images was typically 30 m or better when overlain on georeferenced aerial imagery acquired in 2013 and 2015. Further improvement could be achieved using manual

Figure 11. Mosaic of VNIR imagery acquired along lines 1 through 16 (Fig. 8) in November 2015. This RGB image was constructed from three wavelengths: 485 nm (assigned to blue), 550 nm (assigned to green), and 691 nm (assigned to red).

techniques, but the removal of original image waviness and georeferencing done using an auto-mated approach was sufficient for the preliminary evaluation purposes of this study.

Identifying Mangrove Habitat Using VNIR Data
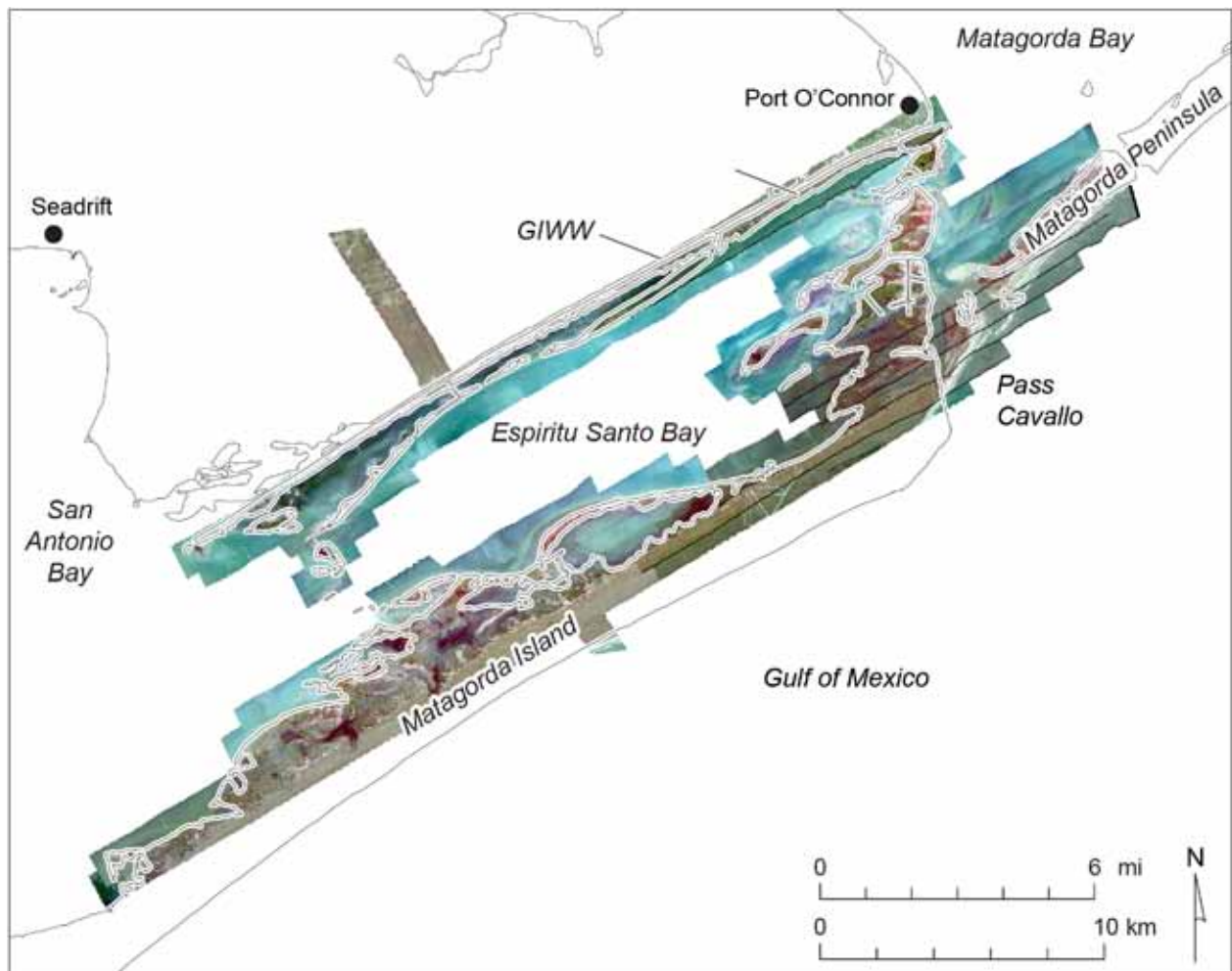
To determine the optimal wavelength bands for discriminating mangrove species in the data set, we first analyzed the average spectral response of different black mangrove regions. Due to the possibility of the motion-compensation algorithm introducing spectral artifacts (because of pixel resampling and interpolation), only the raw spectral data were examined. Five regions were identified in the raw spectral data (Fig. 12). These mangrove sites were confirmed by comparison with a map of mangrove extent as determined through manual analysis of 2013 photographic im-agery and topographic lidar data (Fig. 13). Hand-drawn regions of interest were created for each site using ENVI.
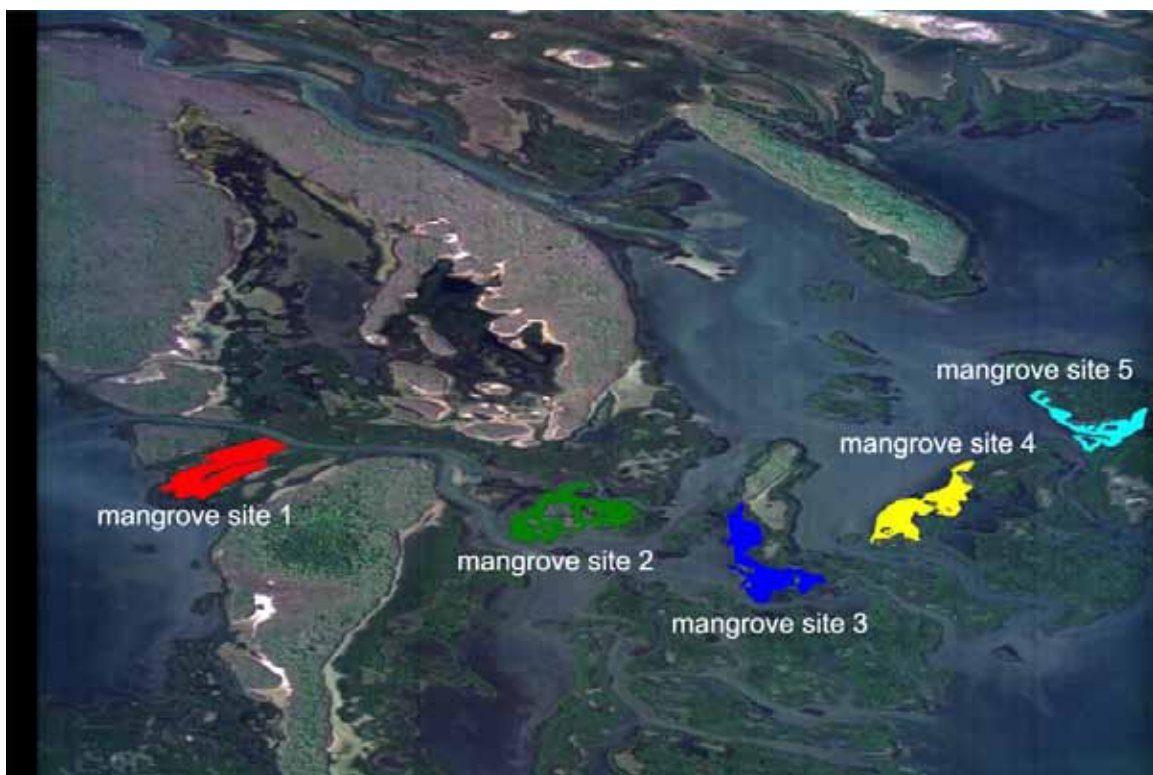

Figure 12. Mangrove sites 1, 2, 3, 4, and 5 identified in the raw VNIR data set.
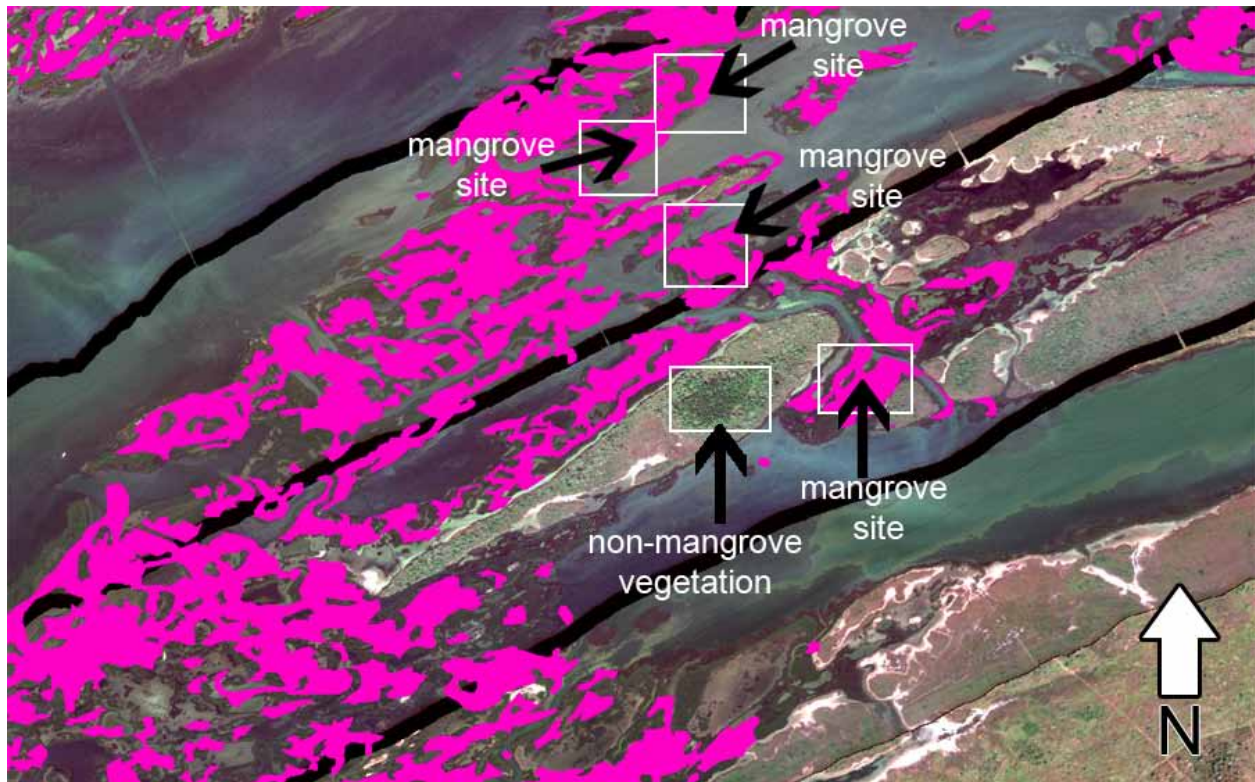
Figure 13. Georectified VNIR image with 2013 mangrove habitat shown in pink.

Preliminary data analysis identified a potential spectral shift along the cross-track direction of the data. Analyses of the average spectral value for each mangrove site confirmed the minor cross-track shift between 580 and 650 nm (Fig. 14). This spectral band was thus excluded from classification. Comparisons of spectral signatures of known mangrove areas with signatures of water, barren tidal flats, low salt marsh, and other habitat (Fig. 15) confirmed that mangroves can be distinguished from most other land-surface types. Nevertheless, some non-mangrove vegetation in the selected regions is spectrally similar to mangroves (Fig. 16). Based on an analysis of average spectral response, the 485, 550, 691, 717, and 800 nm wavelengths were chosen for classification purposes.

The mangrove classification involved two steps: a Normalized Difference Vegetation Index (NDVI) thresholding followed by thresholding the 550-nm wavelength. The NDVI uses the visible and near-infrared bands to assess whether the scene contains live vegetation. NDVI clas-

16

Figure 14. Average spectra of mangrove test sites 1 through 5 (Fig. 12).
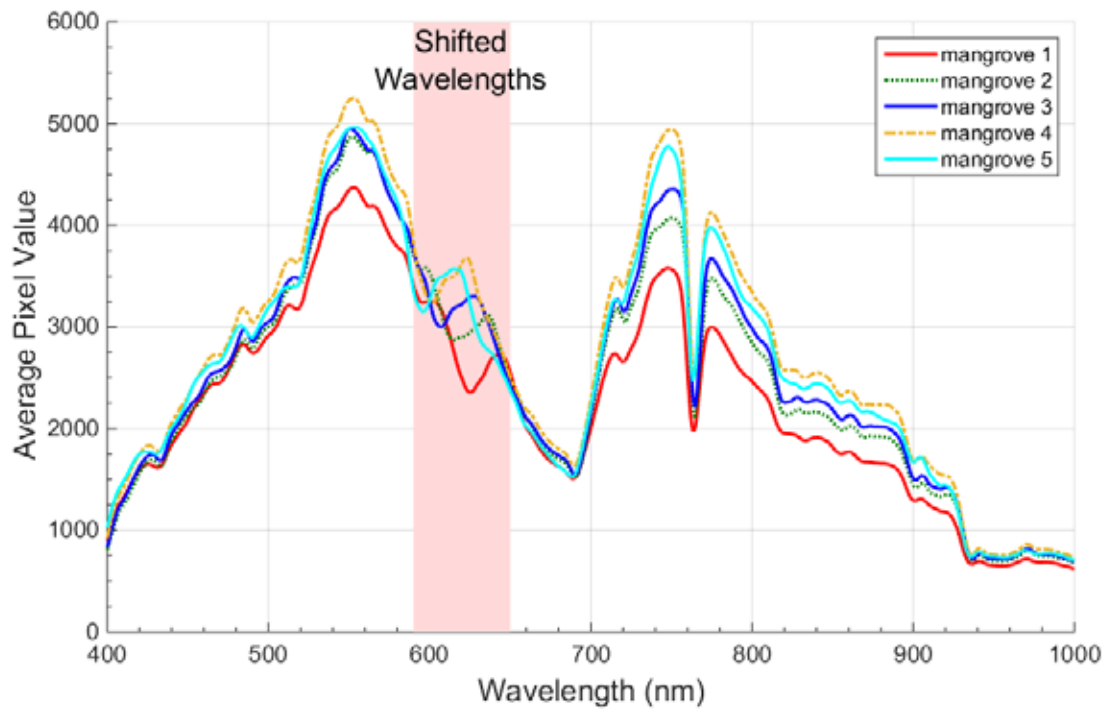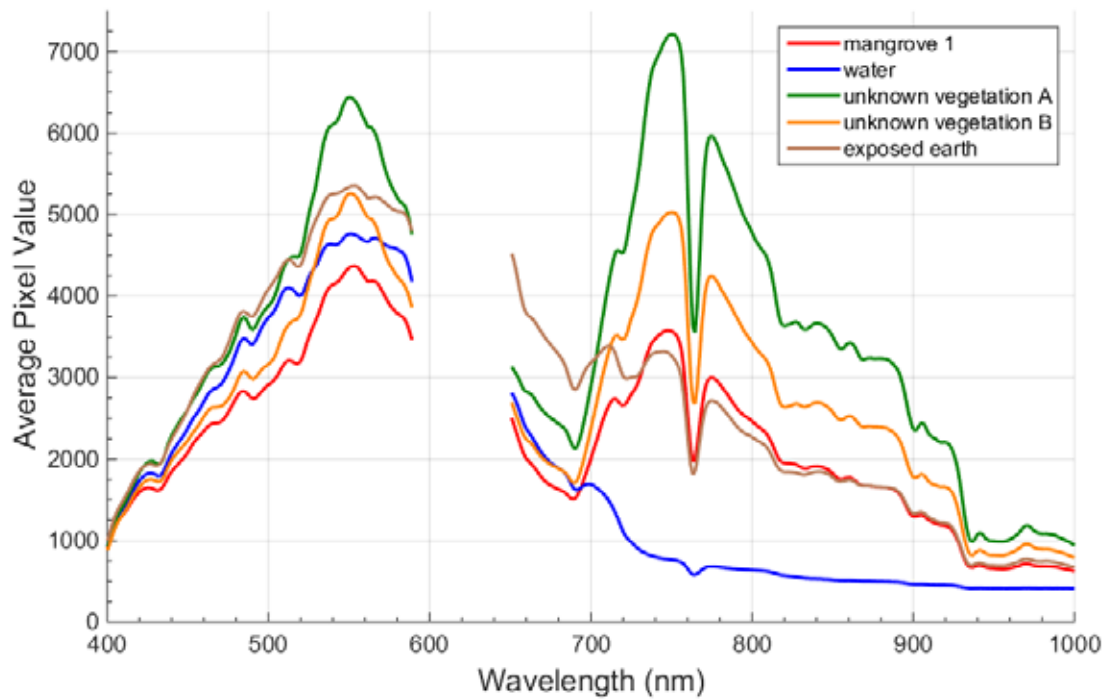

Figure 15. Average spectra of mangrove, water, bare earth, and non-mangrove vegetation areas A and B.
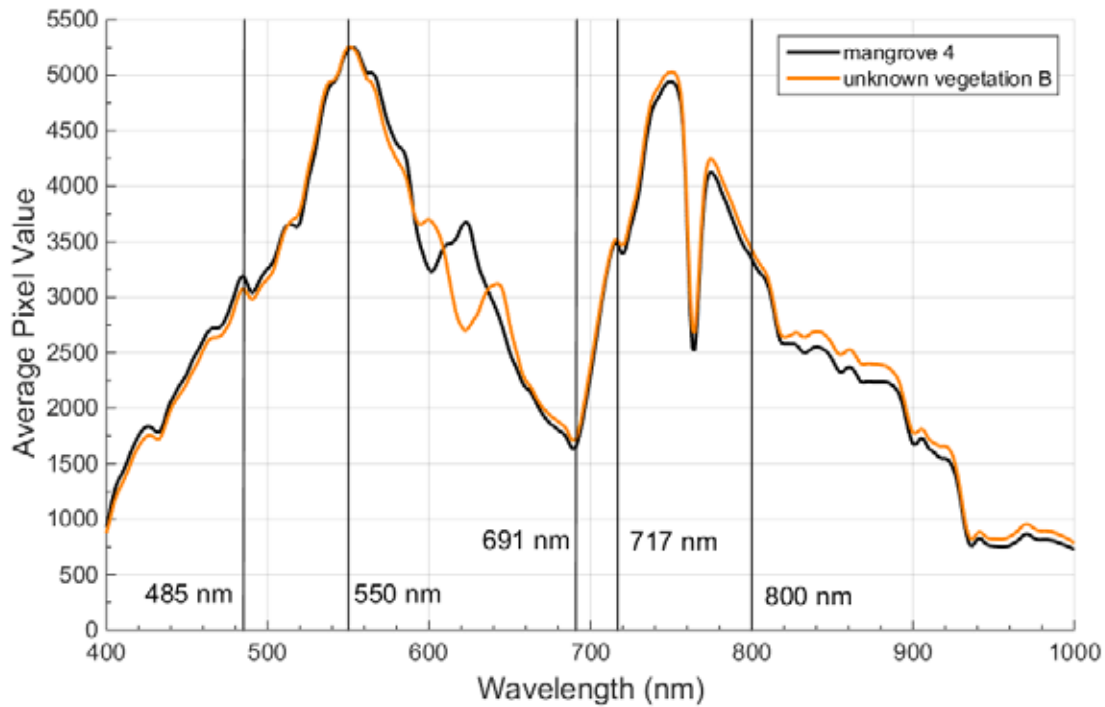
Figure 16. Mangrove (site 4, Fig. 12) and non-mangrove vegetation with identical spectra.

sification uses a ratio along the red edge of vegetation (Equation 1). This resulted in vegetation having large, positive values and all other classes having lower NDVI values. For this study, all NDVI values above 0.2 were classified as vegetation. The 550-nm wavelength was used to separate mangrove from other vegetation identified with the NDVI thresholding. Mangrove spectra were observed to be darker than other vegetation cover types at this wavelength.

$$NDVI = (NIR - red) / (NIR + red) \qquad [Equation\ 1]$$

Using this approach applied to the airborne survey VNIR data, individual pixels were classified as mangrove or not mangrove for seven flight lines with minimal overlap: 2, 4, 6, 8, 10, 12, and 14 (Fig. 8). Polygons were produced for each of those flight lines that enclose the areas classified as mangrove using the VNIR data. The polygons for each flight line were edited, smoothed, and simplified to produce a merged set of polygons within a geographic information system framework.

18

This process identified 12,062 distinct mangrove polygons with a total area of 1,449 ha classified as mangrove from the November 2015 VNIR survey (Fig. 17). Individual areas classified as mangrove ranged from single-pixel size (a few m²) to a maximum individual habitat area of 64 ha.

Preliminary Estimates of Classification Accuracy

Post-classification accuracy was estimated by selecting 75 representative points across the survey area after inspection of the VNIR imagery. This selection was not random; only areas of land
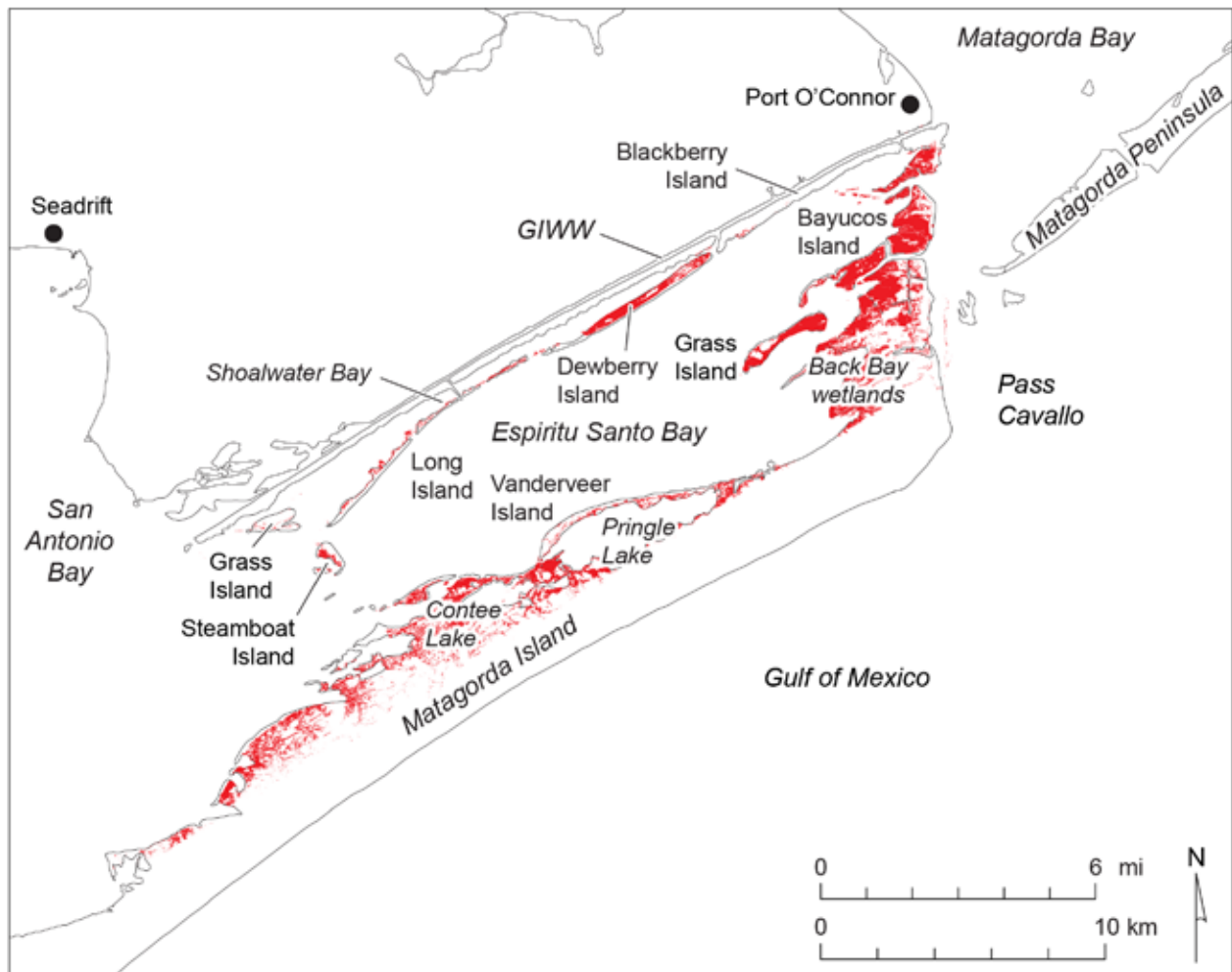
Figure 17. Areas classified as mangrove habitat using VNIR data acquired around Espiritu Santo Bay in November 2015.

or vegetation over water were selected, whereas open water and mainland areas were ignored. When selecting non-mangrove sites, areas of non-mangrove vegetation and bare earth were selected. The classification accuracy at each point was determined by comparing the VNIR-based mangrove classification with manually mapped mangrove distribution on 2013 aerial imagery (Fig. 18) and visual interpretation to determine whether the point was (a) correctly classified as mangrove, (b) correctly classified as non-mangrove, (c) incorrectly classified as mangrove, or (d) incorrectly classified as non-mangrove. The classification accuracy among these four categories was 75 percent.

Figure 18. Map showing manually mapped mangrove distribution in 2013 in the Espiritu Santo Bay area. Mapped areas are classified as E2SS3 according to the Cowardin and others (1979) wetland classification system and were determined during this study from 2013 color-infrared imagery and lidar-derived elevation.

Of the 40 mangrove sites selected, 85 percent were correctly classified as mangrove. The remaining points were areas of patchy mangrove coverage where mangrove was identified in the 5x5-pixel windo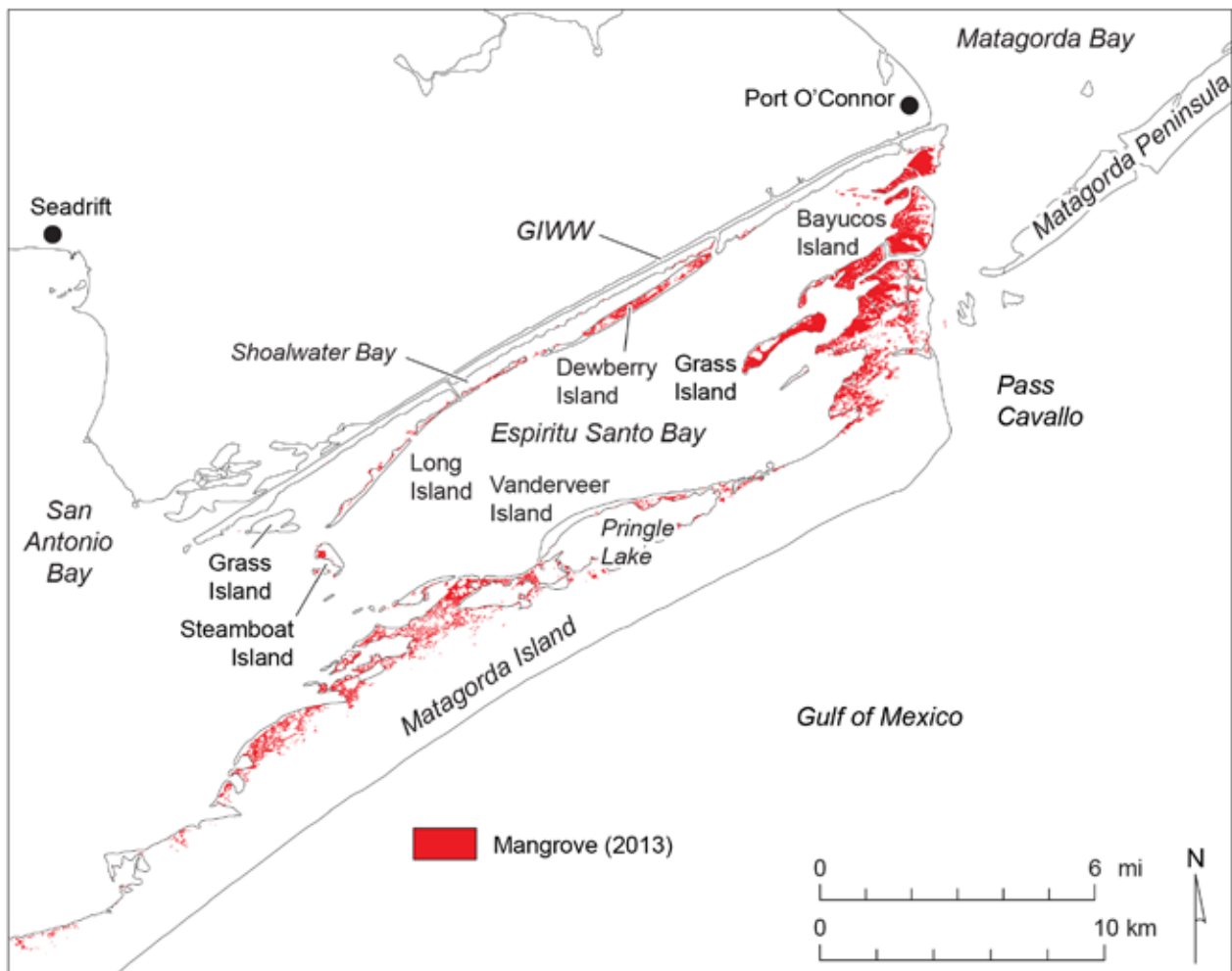w around the sample sites, but not at the sample site. Of the non-mangrove sites examined, 37 percent were incorrectly identified as mangrove, likely because of similarity in spectral signature of mangrove and non-mangrove vegetation in some areas. Many of the erroneously classified mangrove areas were relatively easy to identify using color-infrared imagery and lidar-derived surface elevation and were edited from the final VNIR-based mangrove distribution map (Fig. 17).

Change in Mangrove Habitat Extent Over Time

Comparisons of mangrove distribution within the Espiritu Santo Bay study area from previous studies as well as (a) the manual mangrove distribution determined from 2013 color infrared imagery as ground truth for this study (Fig. 18), and (b) mangrove distribution determined from the airborne hyperspectral data acquired in November 2015 (Fig. 17) show a marked increase in mangrove extent since the 1979 National Wetlands Inventory assessment and since the most recent wetland status and trends studies in the area in the early 2000s.

The first reported occurrence of mangrove on the Texas coast was at the mouth of the Rio Grande in 1853 (Sherrod and McMillan, 1981). Mangrove extent increased between the 1930s and 1979 in three areas of concentration: in the Port Isabel and South Bay area on the southern Texas coast, on Harbor Island between Mustang and San José Islands, and in the Pass Cavallo area along the low tidal-delta islands at between Matagorda Island and Port O'Connor (Sherrod and McMillan, 1981), the area of interest in this survey. Benton and others (1977) state that mangroves occupied 1500 hectares (ha) on the low islands at the time of their remote-sensing survey, but field reconnaissance (Sherrod and McMillan, 1981) indicated that the relative abundance of mangrove and associated *Spartina*, *Batis*, and *Salicornia* varied widely. Maps of mangrove distribution determined from black and white aerial photographs taken in the 1930s and from 1979 color-infrared photographs and field investigations in 1979 and 1980 (Fig. 19) depict a significant increase in
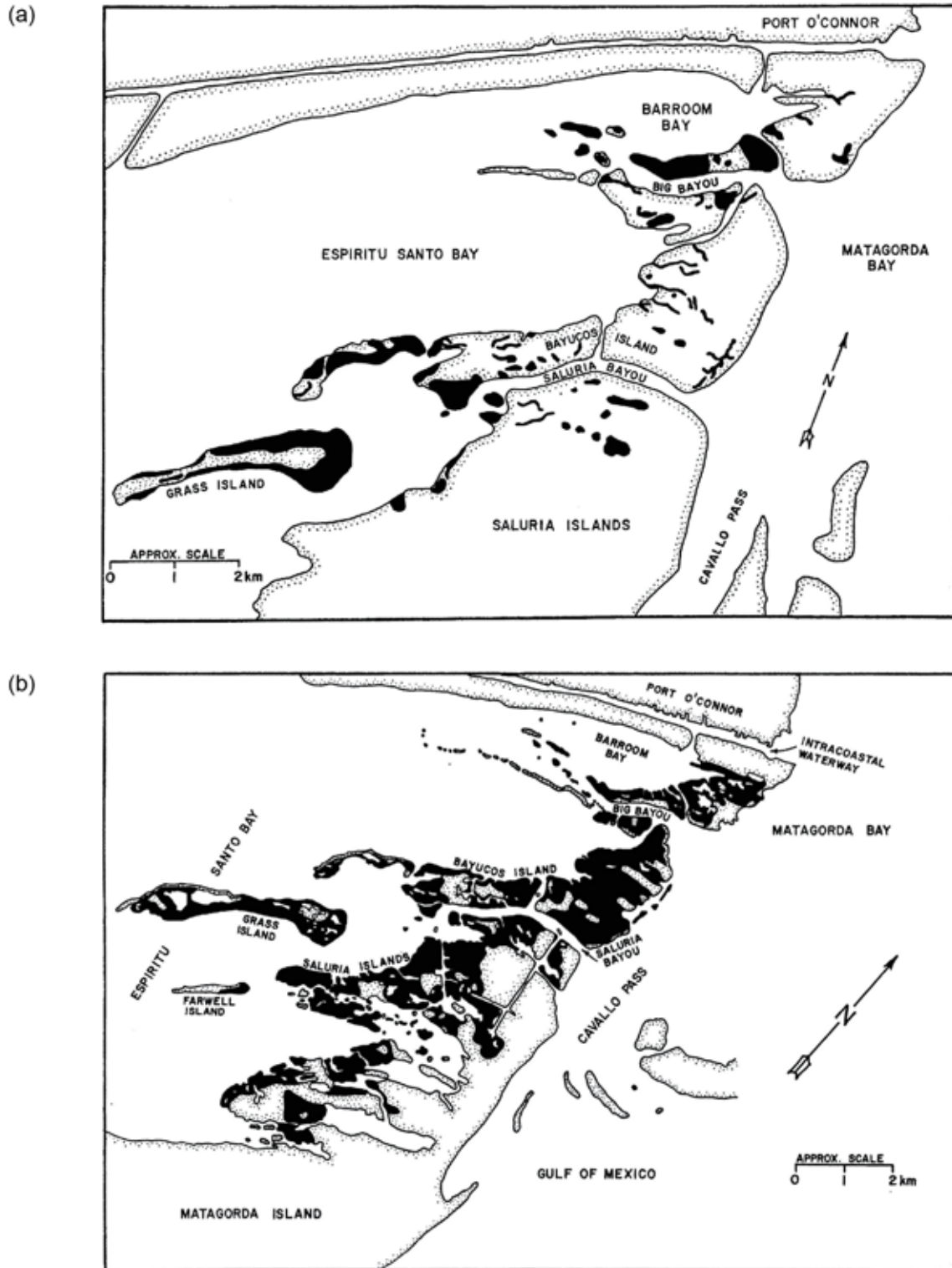
Figure 19. Mapped extent of black mangrove in the Pass Cavallo area (a) in the 1930s and (b) in 1979 based on aerial photographic interpretation and field reconnaissance in 1979 and 1980 (from Sherrod and McMillan, 1981).

mangrove distribution (Sherrod and McMillan, 1981) in the Pass Cavallo area, particularly on Bayucos Island and Saluria Islands. Field investigations in the early 1970s reported the occurrence of black mangrove (as rounded bushes 1 to 2 m high) on the banks of marsh channels and mudflats at the northeast end of Matagorda Island (Hartman and Smith, 1973).

Recent studies of wetlands in the Matagorda Island and Espiritu Santo Bay study area (White and others, 2002) examined aerial photographs from the 1950s (black and white), 1979 (color infrared), and 2001 (color infrared) to obtain estimates of mangrove distribution and change over time. Only very limited areas were interpreted to be occupied by mangroves in the 1950s (4 ha, White and others, 2002), but those classifications were taken only to the class level (E2SS, or estuarine intertidal scrub-shrub) following the system of Cowardin and others (1979) and were hindered by ambiguous expression of mangroves on black-and-white aerial photographs. The mapped extent of estuarine intertidal scrub/shrub wetlands (NWI categories E2SS, E2SSN, and E2SSN/E2FLN), which were considered to be dominantly mangrove, increased to 143 ha based on interpretations of 1979 color infrared imagery (White and others, 2002). Areas classified as dominantly mangrove are located on the low islands along Pass Cavallo between Matagorda Island and Port O'Connor (Fig. 20). Mapping based on 2001 color infrared imagery classified 112 ha as estuarine intertidal scrub/shrub (E2SS3), a classification dominated by black mangrove. As in previous periods, this habitat occurred on the low islands at Pass Cavallo between Matagorda Island and Port O'Connor (Fig. 21). Area classified as mangrove decreased 31 ha between 1979 and 2001, but White and others (2002) note that only areas where black mangrove was dominant were classified as intertidal scrub/shrub. The extent of subdominant mangrove was greater by an unknown amount.

Another likely reason cited by Everitt and Judd (1989), Everitt and others (1996), and White and others (2002) for the decrease in mangrove extent near Port O'Connor between 1979 and 2001 was the occurrence of two major freezes affecting the central Texas coast in 1983 and 1989 (Fig. 22). The 1983 extreme cold period extended from December 22 to 31; record lows were
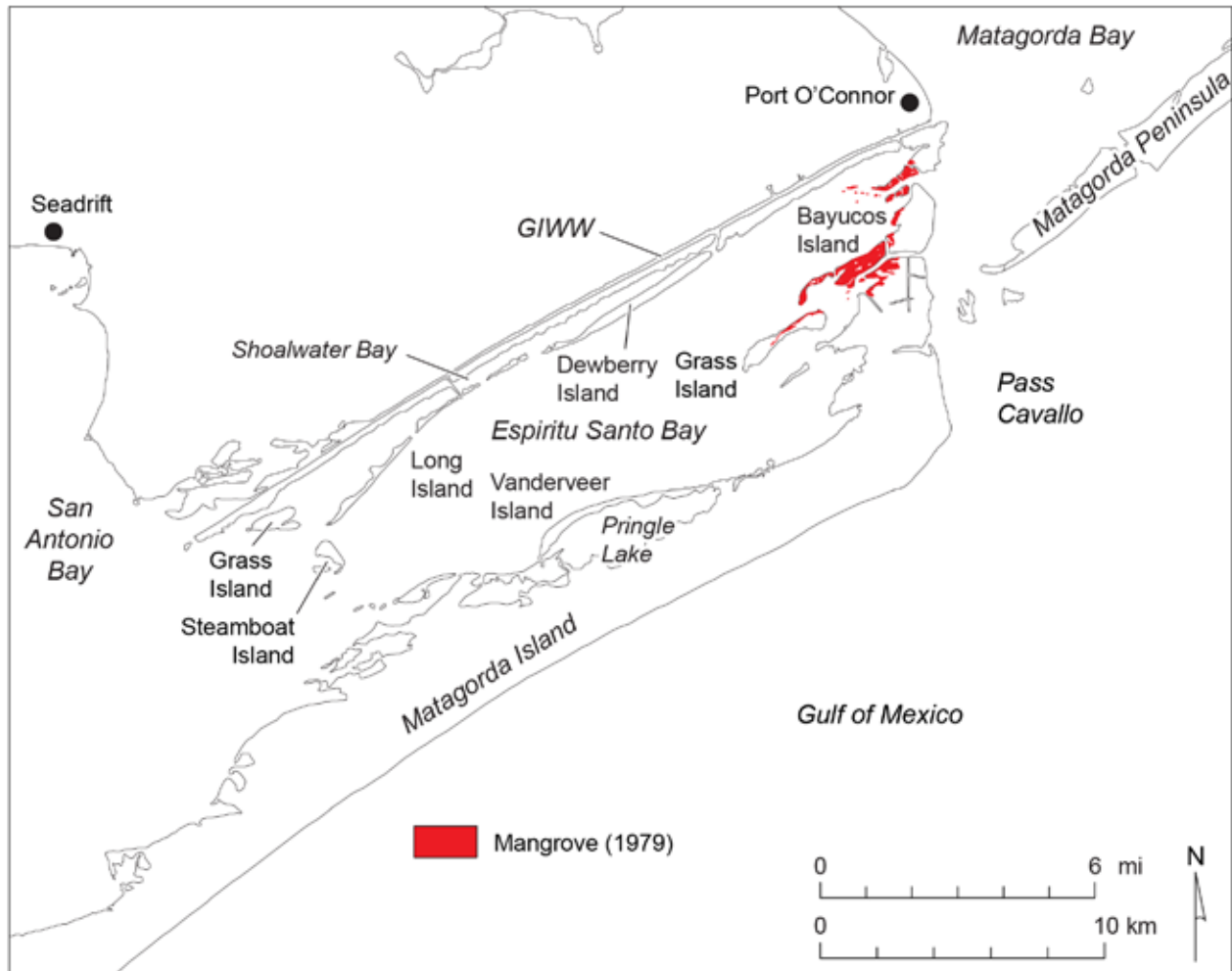
Figure 20. Map showing mangrove distribution in 1979 in the Espiritu Santo Bay area from the National Wetlands Inventory and Shew and others, 1981. Mapped areas are classified as E2SS3N and E2SS3N/E2FLN according to the Cowardin and others (1979) wetland classification system.

set at Rockport, Texas on seven of those days. The lowest temperature at Rockport was -11° C. A second severe and extended freeze occurred from December 22 to 24, 1989, setting two daily record lows at Rockport and again reaching -11° C. Field visits to the Port O'Connor mangrove areas in the late 1980s confirmed that the original mangrove population had been killed by the 1983 freeze and reduced in extent to less than five percent of its pre-freeze extent, but that many young plants had grown from seeds or smaller plants that had been protected from the 1983 freeze (Everitt and Judd, 1989). The surviving mangrove population was again reduced by the
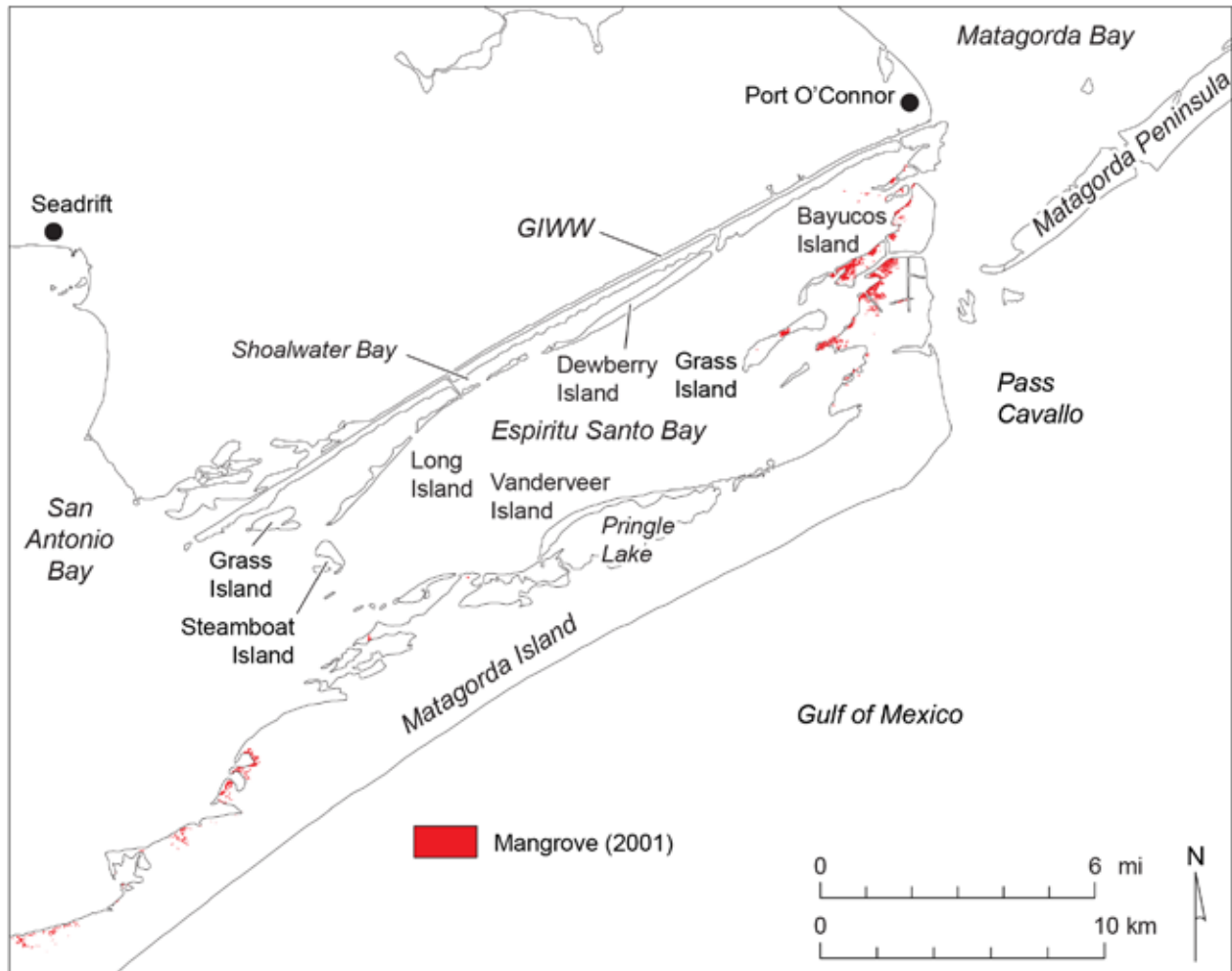
24

Figure 21. Map showing mangrove distribution in 2001 in the Espiritu Santo Bay area (White and others, 2002). Mapped areas are classified as E2SS3 according to the Cowardin and others (1979) wetland classification system.

December 1989 freeze to an area estimated to be less than two percent of that occupied by mangrove before the 1983 freeze (Everitt and others, 1996).

Mangrove mapping conducted in the Espiritu Santo Bay area as ground truth for this study was based on interpretation of color infrared aerial photographs and lidar data acquired in a June 2013 airborne survey of Espiritu Santo Bay (Fig. 18). The color-infrared image (Fig. 23a) displays a distinct spectral response and a textural pattern particular to mangrove. The textural pattern coincides with slightly higher elevation relative to the surrounding marsh habitat (Fig. 23b).
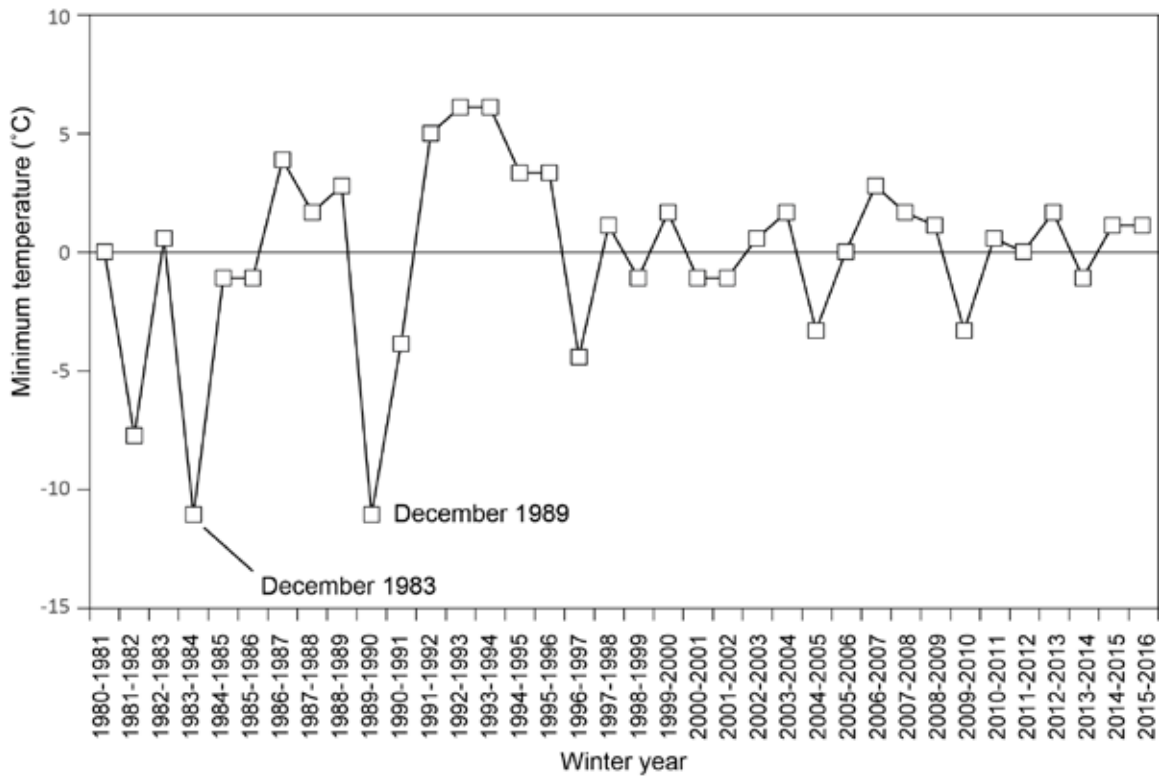
25

Figure 22. Minimum December and January temperatures at the Aransas County Airport (KRKP), Rockport, Texas. Data from National Weather Service.

The mangrove mapping based on 2013 imagery and lidar-derived topography reveals a large increase in the extent of black mangrove since 2001 (Fig. 18), expanding from a mapped area of 112 ha in 2001 (White and others, 2002) to a total area of 1,199 ha in 2013. Mangrove are most extensive on the low islands along Pass Cavallo between Matagorda Island and Port O'Connor, but are also mapped along the bay shoreline of Matagorda Island at Vanderveer Island and on the mainland shore of Espiritu Santo Bay on Dewberry Island, Long Island, and Steamboat Island (Fig. 18). Comparisons of the extent of low salt marsh (estuarine intertidal emergent marsh, unit E2EM1N) mapped in 2001 (Fig. 24a) with the mangrove extent mapped in 2013 (Fig. 24b) indicates that mangrove has become more abundant in low salt marsh habitat. The large increase in areal extent of mangrove between 2001 may reflect growth and spread of young mangrove present but not abundant enough to be mapped separately in 2001. This evident growth and spread
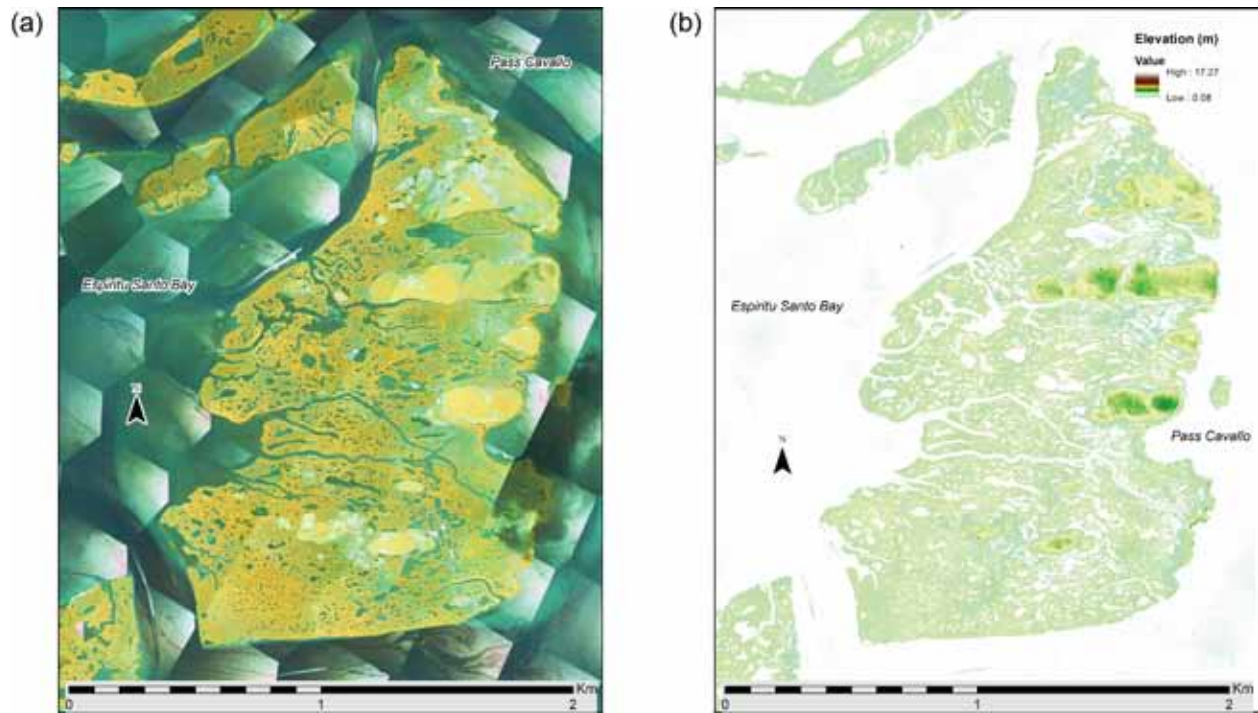
26

Figure 23. (a) Bayucos Island 2013 high resolution color-infrared image and (b) DEM from June 2013 lidar survey.

has been facilitated by the lack of a severe and extended freeze in the area since December 1989 (Fig. 22).

Most change in mangrove habitat occurred in the areas of Bayucos Island and Back Bay Wetlands (Fig. 25). Relative to the overall size of the subarea, Bayucos Island experienced the highest amount of mangrove expansion. The initial area of 50 ha in 2001 increased to 398 ha by 2013, a net gain of 348 ha (Table 3). This represents a nearly 700 percent gain in mangrove habitat at an annual rate of 29 ha per year.

CONCLUSIONS

This preliminary analysis of the application of airborne VNIR surveys to mangrove mapping in the Espiritu Santo Bay area has shown that airborne VNIR data can be acquired, processed, and approximately georeferenced. An automated mangrove mapping approach based on VNIR imagery acquired in November 2015 yielded a total mangrove habitat extent of 1,449 ha, which
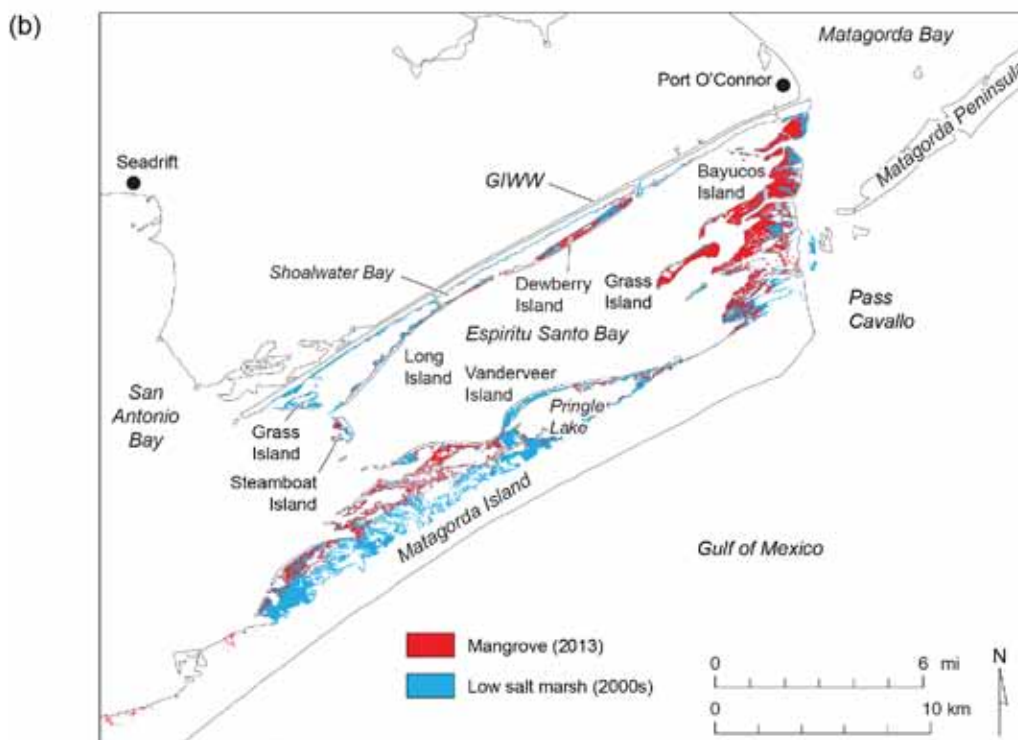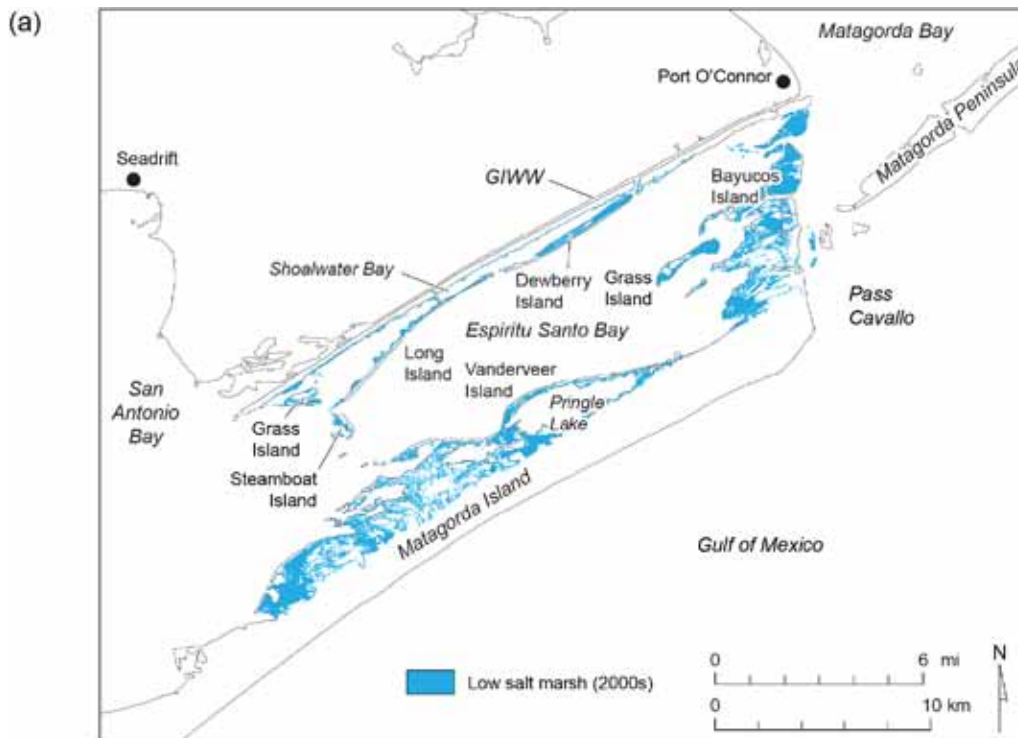
Figure 24. Maps showing replacement of (a) areas mapped as low salt marsh in the early 2000s with (b) areas mapped as mangrove in 2013 (Fig. 18).
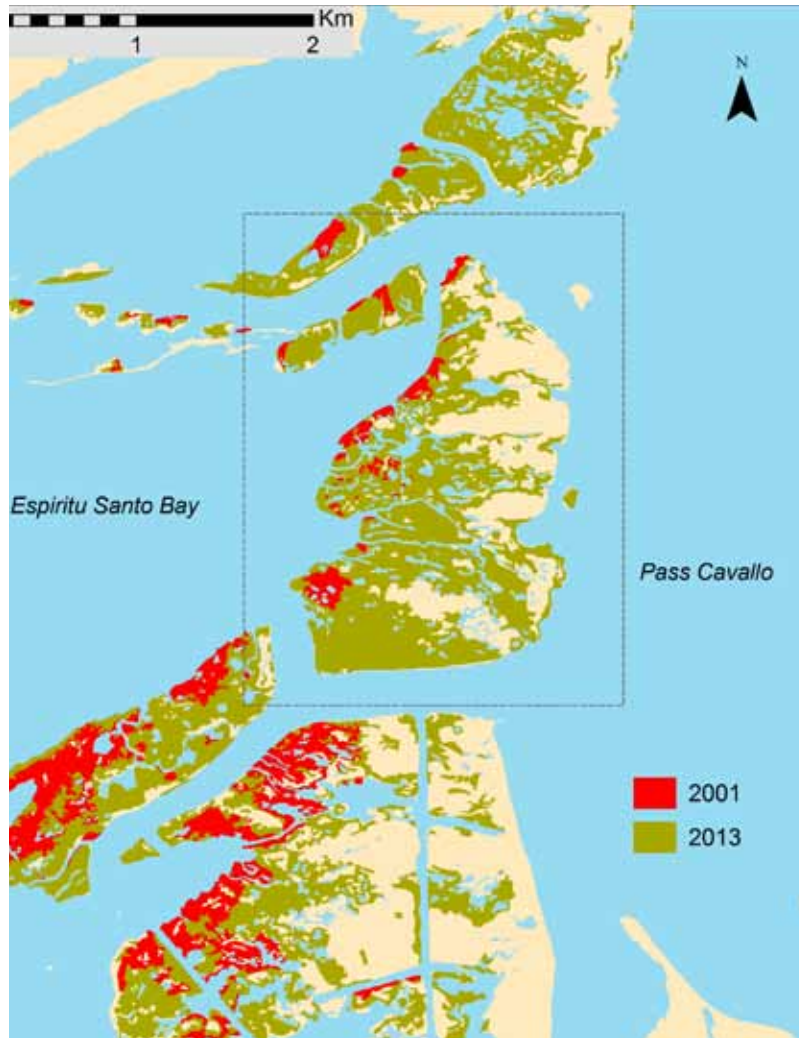
Figure 25. Comparison of 2001 and 2013 mangrove habitat distribution within the Bayucos Island area.

Table 3. Change in mapped mangrove habitat area between 2001 and 2013. Data from White and others (2002) and this study. Locations shown on Fig. 2.

Area	2001 area (ha)	2013 area (ha)	Change (ha)
Bayucos Island	50	398	348
Back Bay wetlands	60	367	307
Contee Lake-Vanderveer Island	20	328	308
Dewberry Island		80	80
Shoalwater Bay		23	23
Blackberry Island		2	2
Total	130	1,199	1,068

is similar to, but about 20 percent greater than the 1,199 ha extent mapped manually from color infrared aerial photographs and lidar-derived topographic data acquired in 2013, two years before the VNIR survey. Both approaches suggest that mangrove habitat has expanded in the area since previous inventories based on 1979 and 2001 aerial photographs, although the total extent of mangrove in those inventories may be underrepresented by the use of a more restrictive threshold of mangrove dominance. The 2013 and 2015 determinations of mangrove extent are similar to estimates from the mid-1970s that were likely less restrictive, before two severe and extended freezes in 1983 and 1989 greatly reduced mangrove extent in the Espiritu Santo Bay area.

Advantages of the VNIR-based approach to mangrove mapping include the achievable mapping resolution of a few square meters and the ability to discriminate small mangrove and non-mangrove habitat at reasonable accuracy that would be very labor-intensive to map manually. Principal disadvantages encountered during this initial study include (1) difficulty in georeferencing scan-based VNIR imagery to accuracy levels achieved with airborne lidar and frame-based aerial photography, and (2) difficulty acquiring robust and consistent VNIR data in coastal areas where parameters that affect spectral response (including humidity, tidal conditions, soil and water salinity, and vegetation condition) can change at hourly, daily, seasonal, and annual time scales.

ACKNOWLEDGMENTS

computer applications to georeference and export the VNIR data for analysis. Rebecca Brown processed the airborne survey data and developed an approach to identify mangrove habitat from VNIR data, with assistance from John R. Andews, Kutalmis Saylam, and Aaron Averett. Thomas A. Tremblay mapped the 2013 distribution of mangroves. Jeffrey G. Paine and Thomas A. Tremblay provided historical mangrove context. Rebecca Brown, Jeffrey G. Paine, Thomas A. Tremblay, and Kutalmis Saylam contributed to the report.

REFERENCES

Adam, E., Mutanga, O., and Rugege, D., 2010, Multispectral and hyperspectral remote sensing for identification and mapping of wetland vegetation: a review: Wetlands Ecology and Management, 18(3), 281-296.

Armitage, A. R., Highfield, W. E., Brody, S. D., and Louchouarn, P., 2015, The contribution of mangrove expansion to salt marsh loss on the Texas Gulf Coast: PLoS ONE , 10(5):e0125404; doi:10.1371/journal.pone.0125404.

Aspinall, R. J., Marcus, W. A., and Broadman, J. W., 2002, Considerations in collecting, processing, and analysing high spatial resolution hyperspectral data for environmental investigations: Journal of Geographical Systems, 4(1), 15-29.

Benton, A. R., Hatch, S. L., Kirk, W. L., Newman, R. M., Snell, W. W., and Williams, J. G., 1977, Monitoring of Texas coastal wetlands: College Station, Texas, Texas A&M University, Remote Sensing Center Technical Report RSC-88.

Blasco, F., Aizpuru, M., and Din Ndongo, D., 2005, Mangroves, Remote Sensing: in Encyclopedia of Coastal Science: Springer Science and Business Media, p. 614-618.

Blasco, F., Gauquelin, T., Rasolofoharinoro, M., Denis, J., A. M., and Caldairou, V., 1998, Recent advances in mangrove studies using remote sensing data: Marine and Freshwater Research, 49(4), 287-296.

Christian, B., and Krishnayya, N., 2009, Classification of tropical trees growing in a sanctuary using Hyperion (EO-1) and SAM algorithm: Current Science, p. 1601-1607.

Coates, C., Fowler, B., and Holst, G., 2009, sCMOS Scientific CMOS technology: A high-performance imaging breakthrough: White paper, Andor Technology, Fairchild Imaging and PCO AG.

Cowardin, L. M., Carter, V., Golet, F. C., and LaRoe, E. T., 1979, Classification of wetlands and deepwater habitats of the United States: Washington, D. C., U.S. Department of the Interior, Fish and Wildlife Service, 131 p.

Dell'Endice, F., Nieke, J., Koetz, B., Schaepman, M., and Itten, K., 2009, Improving radiometry of imaging spectrometers by using programmable spectral regions of interest: ISPRS Journal of Photogrammetry and Remote Sensing, 64(6), 632–639.

Elowitz, R. M., undated, "What is Imaging Spectroscopy (Hyperspectral Imaging)?": http://www.markelowitz.com/Hyperspectral.html.

Everitt, J. H., and Judd, F. W., 1989, Using remote sensing techniques to distinguish and monitor black mangrove (*Avicennia germinans*): Journal of Coastal Research, v. 5, no. 4, p. 737-745.

Everitt, J. H., Judd, F. W., Escobar, D. E., and Davis, M. R., 1996, Integration of remote sensing and spatial information technologies for mapping black mangrove on the Texas Gulf Coast: Journal of Coastal Research, v. 12, p. 64-69.

Green, E. P., Mumby, P. J., Edwards, A. J., Clark, C. D., and Ellis, A. C., 1998, The assessment of mangrove areas using high resolution multispectral airborne imagery: Journal of Coastal Research, v. 14, no. 2, p. 433-443.

Guo, H., Zhang, Y., Lan, Z., and Pennings, S., 2013, Biotic interactions mediate the expansion of black mangrove (*Avicennia germinans*) into salt marshes under climate change: Global Climate Change, p. 2765-2774.

Hartman, R. L., and Smith, J., 1973, A floristic and ecological study of Matagorda Island: in Matagorda Isalnd: A Natural Area Survey: LBJ School of Public Affairs, The University of Texas at Austin, Part II, p. 116-145.

Hirano, A., Madden, M., and Welch, R., 2003, Hyperspectral image data for mapping wetland vegetation: Wetlands, p. 436-448.

Jensen, J. R., 2007, Remote sensing of vegetation: in Remote Sensing of the Environment: An Earth Resource Perspective: Prentice Hall, p. 355-408.

Klemas, V. V., 2015, Remote Sensing of Mangroves. in Tiner, R. W., Lang, M. W, and Klemas, V. V., editors, Remote Sensing of Wetlands: Applications and Advances: CRC Press, p. 243-263.

Lang, M. W., and McCarty, G. W., 2008, Remote sensing data for regional wetland mapping in the United States: trends and future prospects: in Wetlands: Ecology, Conservation and Restoration, Nova Science Publishers, p. 73-112.

Richardson, A., and King, K., 2011, Dicots (Dicotyledoneae): in Plants of Deep South Texas: a Field Guide to the Woody and Flowering Species: College Station, Texas, Texas A&M University Press, p. 48-427.

Rundquist, D. C., Narumalani, S., and Narayanan, R. M., 2001, A review of wetlands remote sensing and defining new considerations: Remote Sensing Reviews, v. 20, no. 3, p. 207-226.

Schowengerdt, R. A., 2007, Correction and calibration: in Remote Sensing: Models and Methods for Image Processing: Burlington, MA, Academic Press, p. 285-253.

Sherrod, C. L., and McMillan, Calvin, 1981, Black mangrove, *Avicennia germinans*, in Texas: past and present distribution: Port Aransas, Texas, The University of Texas Marine Science Institute, Contributions in Marine Science, v. 24, p. 115-131.

Shew, D. M., Baumann, R. M., Fritts, T. H., and Dunn, L. S., 1981, Texas barrier island region ecological characterization: environmental synthesis papers: Washington, D.C., U.S. Department of the Interior, Fish and Wildlife Service, Office of Biological Services, FWS/

OBS-81/32, 413 p.

Smith, G. M., and Milton, E. J., 1999, The use of the empirical line method to calibrate remotely sensed data to reflectance: International Journal of Remote Sensing, v. 20, no. 13, p. 2653-2662.

Spalding, M., Kainuma, M., and Collins, L., 2010a, Mangrove ecosystems: in World Atlas of Mangroves, Earthscan, p. 1-22.

Spalding, M., Kainuma, M., and Collins, L., 2010b, North and Central America and the Caribbean: in World Atlas of Mangroves, p. 181-214.

Staben, G. W., Pfitzner, K., Bartolo, R., and Lucieer, A., 2012, Empirical line calibration of WorldView-2 satellite imagery to reflectance data: using quadratic prediction equations: Remote Sensing Letters, 2(6), 521-530.

U.S. Fish and Wildlife Service, 1983, Unpublished digital data of wetland maps of the Texas coastal zone prepared from mid-1950's and 1979 aerial photographs: Washington, D. C., U.S. Department of the Interior, Fish and Wildlife Service, Office of Biological Services.

Vaiphasa, C., Ongsomwang, S., Vaiphasa, T., and Skidmore, A. K., 2005, Tropical mangrove species discrimination using hyperspectral data: A laboratory study: Estuarine, Coastal and Shelf Science, v. 65, no. 1, p. 371-379.

Wang, L. E., and Sousa, W. P., 2009, Distinguishing mangrove species with laboratory measurements of hyperspectral leaf reflectance: International Journal of Remote Sensing, v. 30, no. 5, p. 1267-1281.

White, W. A., Tremblay, T. A., Waldinger, R. L, and Calnan, T. R., 2002, Status and trends of wetland and aquatic habitats on Texas barrier islands, Matagorda Bay and San Antonio Bay: The University of Texas at Austin, Bureau of Economic Geology, final report prepared for the Texas General Land Office and National Oceanic and Atmospheric Administration under GLO Contract No. 01-241-R, 66 p.

Yang, C., Everitt, J. H., Fletcher, R. S., Jensen, R. R., and Mausel, P. W., 2009, Evaluating AISA+ hyperspectral imagery for mapping black mangrove along the South Texas Gulf Coast: Photogrammetric Engineering and Remote Sensing, v. 75, no. 4, 425-435.

Zhang, C., Kovacs, J. M., Liu, Y., Flores-Verdugo, F., and Flores-de-Santiago, F., 2014, Separating mangrove species and conditions using laboratory hyperspectral data: A case study of a degraded mangrove forest of the Mexican Pacific: Remote Sensing, v. 6, no. 12, p. 11673-11688.

Page intentionally blank

Summary of ground-based spectral data acquired around Espiritu Santo Bay on November 18, 2015 (the first day of the airborne survey with the VNIR camera). All data were acquired with a ASD FieldSpec 4 spectroradiometer at the times listed below.

Table A1. Location number (Fig. 2), latitude and longitude (in decimal degrees, WGS84 datum), measurement time (U.S. Central Standard Time), number of measurements, and target feature for FieldSpec 4 spectral measurements.

| Location	Latitude	Longitude	Time (CST)	Samples	Feature
1	28.31087	-96.62516	9:59 to 10:01	4	Black mangrove (leaf)
1	28.31087	-96.62516	10:07 to 10:08	4	Black mangrove
2	28.30317	-96.61956	10:24 to 10:26	6	Black mangrove
3	28.28344	-96.60761	10:35 to 10:42	6	Black mangrove
4	28.29654	-96.59266	10:57 to 10:58	4	Black mangrove
5	28.30158	-96.57176	11:12 to 11:14	6	Black mangrove
6	28.42434	-96.41661	13:06 to 13:11	4	Black mangrove
7	28.42150	-96.41324	13:24 to 13:27	4	Black mangrove
7 to 8	na	na	13:37 to 13:38	2	Smooth cordgrass
7 to 8	na	na	13:38	1	Black mangrove
8	28.37699	-96.45730	14:01 to 14:06	3	Black mangrove
9	28.37745	-96.45807	14:15 to 14:16	4	Water
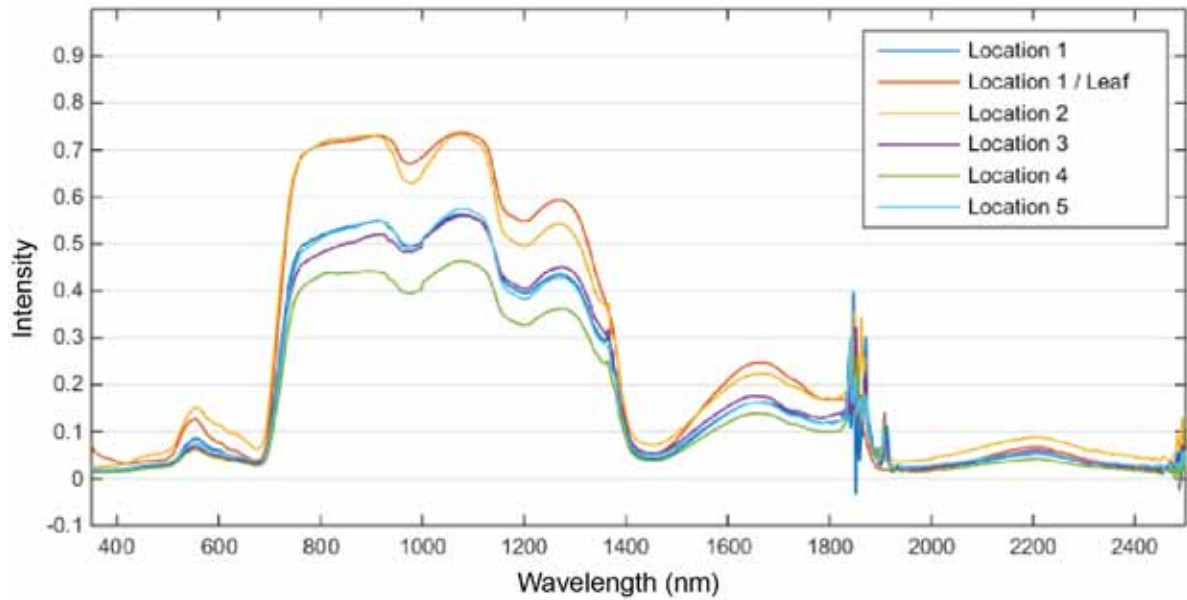
Figure A1. Spectroradiometer intensity measured on black mangroves (*Avicennia germinans*) at locations 1 through 5, southwestern Espiritu Santo Bay (Fig. 2, Table A1).
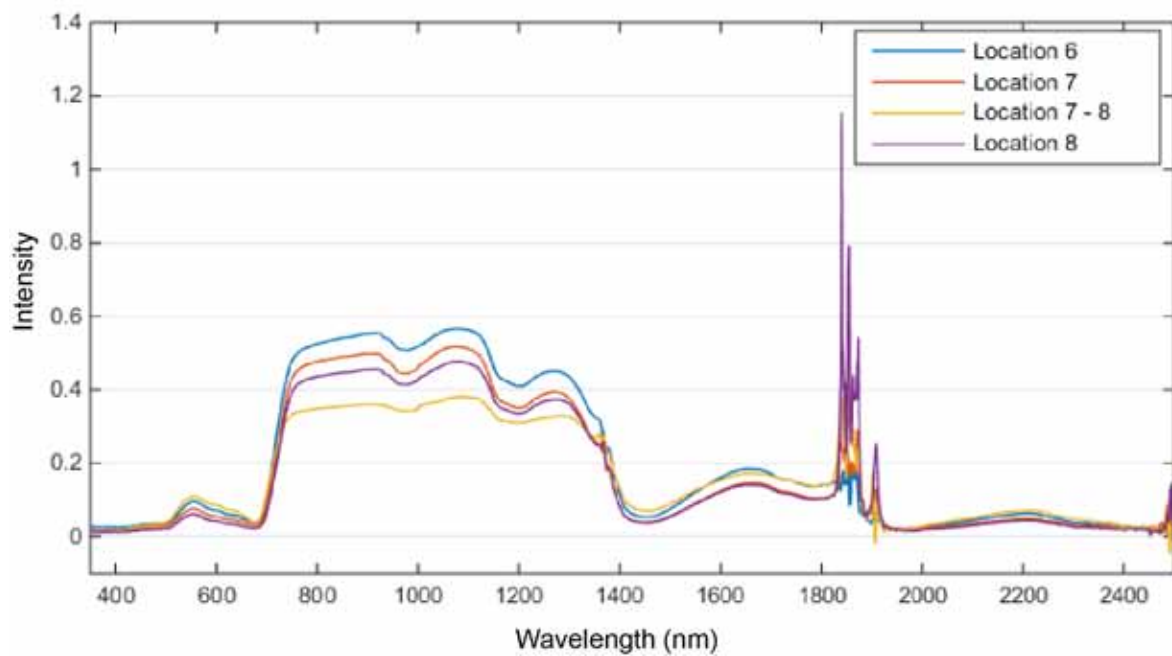

Figure A2. Spectroradiometer intensity measured on black mangroves at locations 6, 7, and 8, northeastern Espiritu Santo Bay (Fig. 2, Table A1).
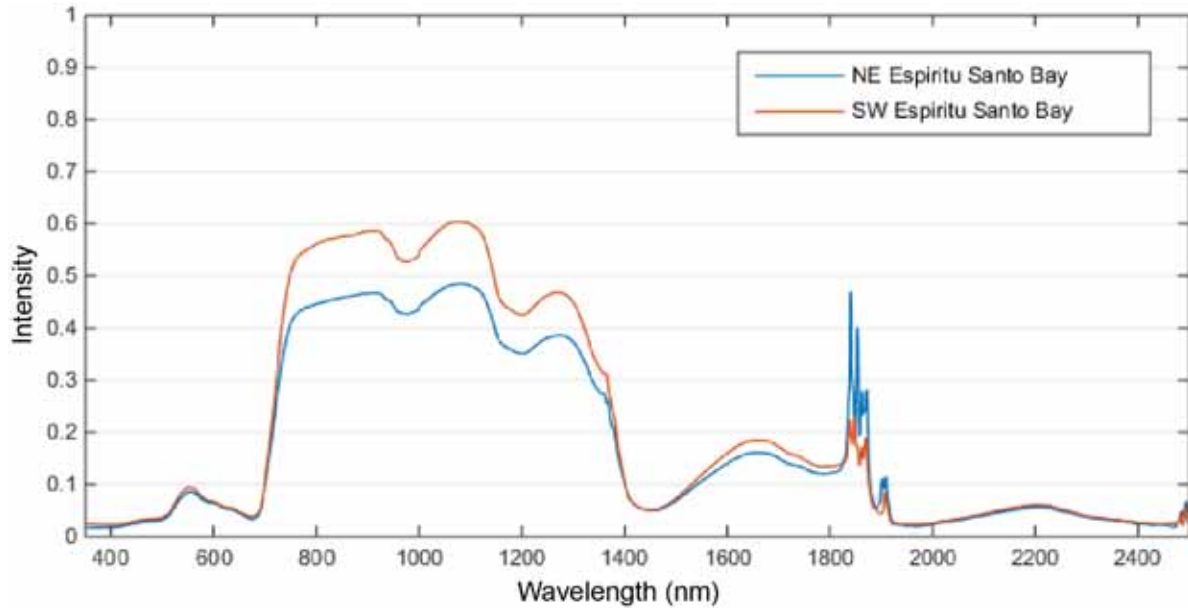
Figure A3. Average spectroradiometer intensity measured on black mangroves (*Avicennia germinans*) in northeastern and southwestern Espiritu Santo Bay.
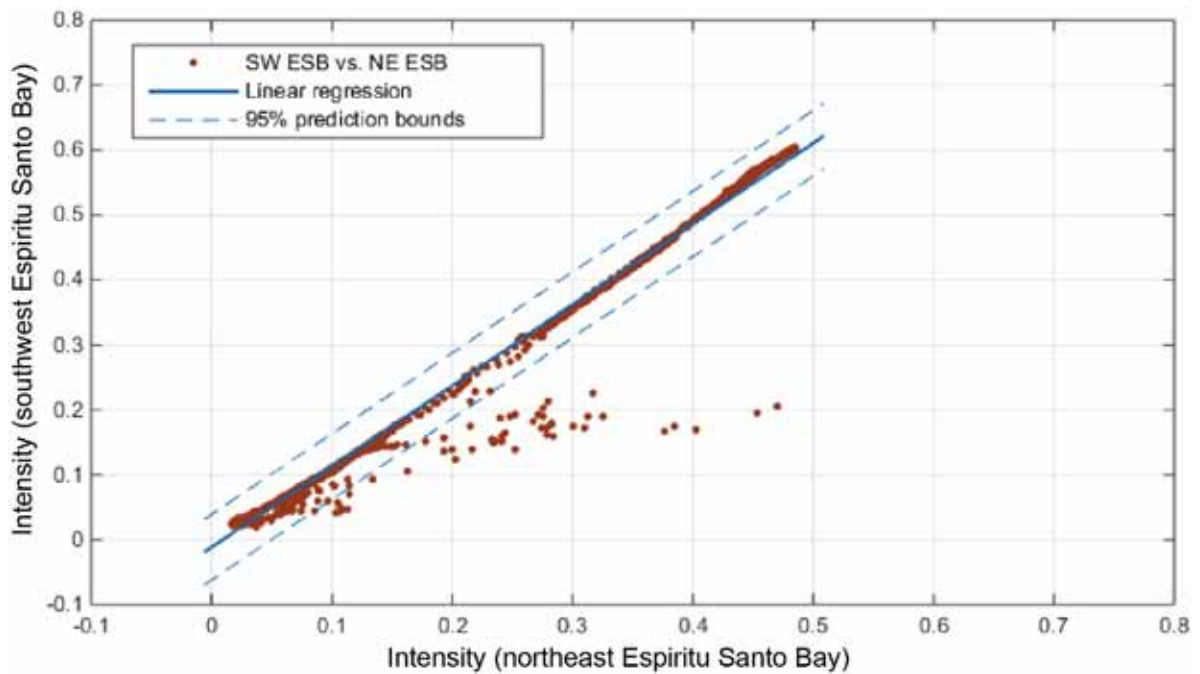

Figure A4. Relationship between spectral intensity measured for black mangrove in northeastern Espiritu Santo Bay and southwestern Espiritu Santo Bay.
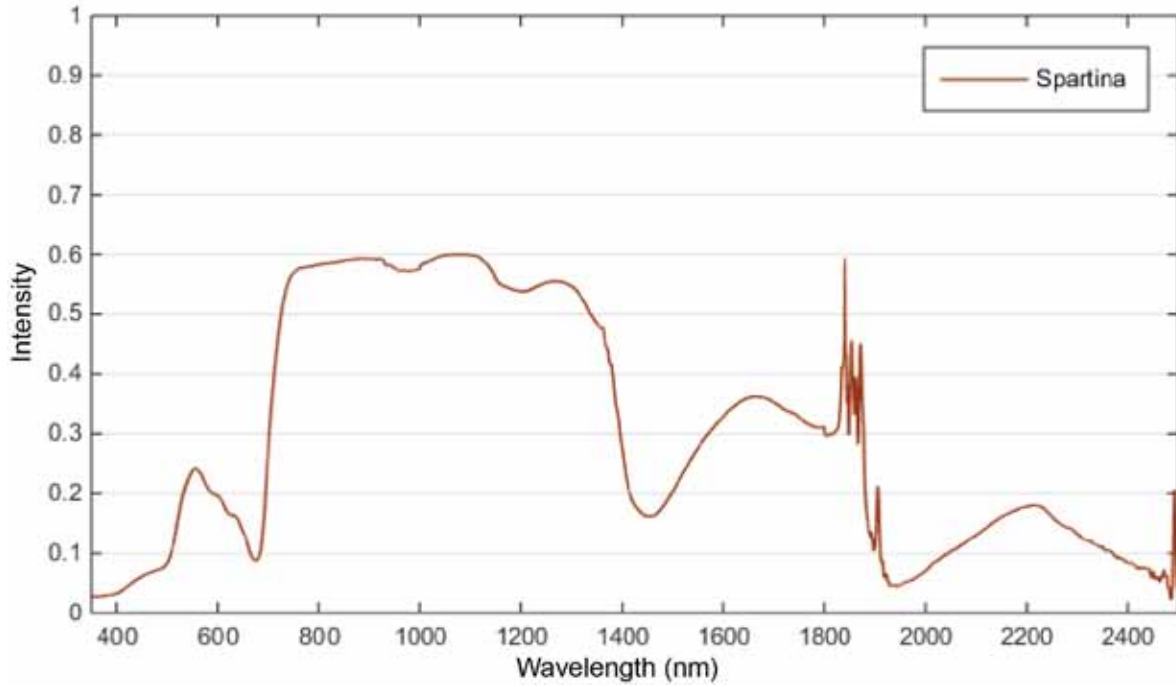
Figure A5. Spectroradiometer intensity measured on smooth cordgrass (*Spartina alterniflora*) between locations 7 and 8, northeastern Espiritu Santo Bay (Fig. 2, Table A1).
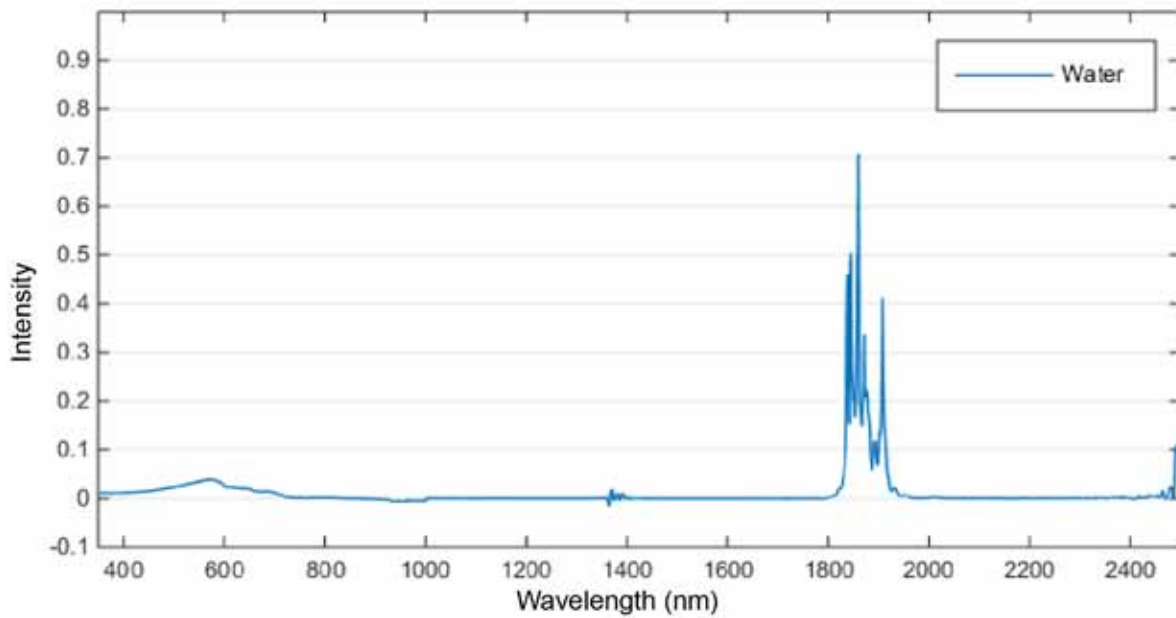

Figure A6. Spectroradiometer intensity measured on bay water, location 9, northeastern Espiritu Santo Bay (Fig. 2, Table A1).

GeoFORCE TEXAS

9th Grade Academy

Fourth Edition

THE UNIVERSITY OF TEXAS AT AUSTIN

JACKSON

SCHOOL OF GEOSCIENCES

SWTJC
Southwest Texas Junior College

HOUSTON
Independent School District
Creating a College-Bound Culture

THE UNIVERSITY OF TEXAS AT AUSTIN

GeoFORCE TEXAS

9th Grade Academy

Guidebook for Geoscience Field Trip
Austin, Port Aransas, and Galveston, Texas

First Edition, 2009
Second Edition, 2012
Third Edition, 2013

by
Tiffany Caudle,* Jay Raney,** and
Sigrid Clift**

Revised 2016

*Tiffany Caudle is a geologist at the
Bureau of Economic Geology
Scott W. Tinker, Director
A research unit of the Jackson School of Geosciences.

**Jay Raney and Sigrid Clift are advisors to the GeoFORCE
Texas program.

Table of Contents

Day #3
AUSTIN, TEXAS, TO PORT ARANSAS, TEXAS

Orientation

Where are we, what will we see? Today we drive to Port Aransas on Mustang Island, a barrier island. We will have one field stop at Goose Island State Park followed by swimming in the Gulf of Mexico.

Coastal Texas is flat, it's hot and humid, and it has great beaches but very little shade. We'll spend quite a bit of time on the beach, in wetlands, and on tidal flats over the next few days. Drink lots of water to stay hydrated, wear sunscreen to protect your skin, and a hat would be helpful to shade your eyes.

> **Study hint:** There will be a quiz this evening. It may have questions on last night's lectures and topics related to what we will see at Goose Island State Park that are described in the next pages of the guidebook. The time spent riding the bus to the coast is a good chance to read the guidebook. The more reading you do now, the less late-night studying you'll have to do later.

What will we learn about today? The trip itself is a learning experience. Seeing new places, maybe meeting new people—anytime you do something new you learn new things. A lot of what you learn in GeoFORCE isn't in the guidebook, it's what you absorb from the experience. Travel opens us up and gives us new perspectives. It reminds us that the world is a very big place. Travel broadens our outlook, and that's a good thing.

We'll also learn some geology today. We will stop at Goose Island State Park to discuss bays and estuaries. And tonight our hotel is on a barrier island on the Gulf of Mexico. We'll go to the beach and begin to learn about barrier islands and the geologic processes that are active on the coast. We will also spend some time relaxing and enjoying the beaches and waters of the Gulf of Mexico.

Today's geo-word: There will be no new geo-words during today's field stop.

Stop #5
GOOSE ISLAND STATE PARK

Our first stop this moring will be at Goose Island State Park on the shores of Aransas Bay and St. Charles Bay (look for the red dot on **fig. 72**). The land for the park was acquired by the state between 1931-1935. The land had preciously been privately owned. The Civilian Conservation Corps built the earliest park facilities in the 1930's.

> **Did you know?** The Civilian Conservation Corps (CCC) was a public work relief program that was part of President Frankin D. Roosevelt's New Deal. The CCC was designed to provide unskilled manual labor jobs to young men who were unable to find jobs due to the Great Depression in the United States. The jobs were related to converation and development of natural resources on lands owned by federal, state, and local governments. The CCC provided the men with shelter, clothing, food, and small wage. The program also established a national awareness of protecting and conserving the nation's natural resources.

The stop this morning is to further discuss the importance of bays and estuaries environments to the Texas coast. Aransas Bay (just like Galveston Bay from our lecture last night) is a network of bays and estuaries. Look at the image in **figure 72**. Copano Bay and Mission Bay are to the west, Redfish Bay is to the south, St. Charles Bay stretches to the north, and Mequite Bay is connected to the northeast. Freshwater is fed to the estuaries by the Mission and Aransasa Rivers as well as numerous small streams.

Where is the outlet to the Gulf of Mexico for this bay system? Aransas Pass, which separates Mustang Island and San Jose Island, was for

Figure 72. Copano/Aransas Bay system on the Texas coast. The red dot marks the location of Goose Island State Park.

many years the only continious connection to the Gulf of Mexico for the Copano and Aransas Bays system.

Look again at **figure 72**. Do you see Cedar Bayou? Cedar Bayou is a small natural tidal inlet that separates San Jose Island from Matagorda Island to the north. The inlet was closed in 1979 to protect Mesquite Bay from an oil spill in the Gulf of Mexico. Since than it has been opened occasionally by storms or dreging but the opening quickly filled with sediments. Recently, a large effort was undertaken to restore and open the pass for good in an effort to increase circulation of marine waters from the Gulf into the bay system, particularly Mesquite Bay.

A healthy bay system is very important for fish habitat, wetlands, oyster beds, migratory birds, and endangered species. In an effort to help protect and to learn more about the environments of the Copano and Aransas Bays system, the bays have been included in the Mission-Aransas National Estuarine Research Reserve (NERR). Habitats found in the Mission-Aransas NERR include tidal flats, seagrass beds, mangroves, and oyster reefs. The site also serves as the winter home (Aransas National Wildlife Refuge) to the critically endangered Whooping Crane (**fig. 73**).

Did you know? In 1941 there were only 15 surviving Whooping Cranes that all belonged to one flock that migrated between Wood Buffalo National Park in Canada and the Aransas National Wildlife Refuge in Texas! The migratory route is about 2,500 miles. Due to conservation efforts, there were an estimated 308 whooping cranes that wintered in the Aransas National Wildlife Refuge in 2014-15. Adult Whooping Cranes stand 5 feet tall, weigh 15 pounds, and have a wingspan of more than 7.5 feet!

Mangroves and Whooping Cranes: An area of research that is taking place along the shorelines of several Texas bays (Aransas Mesquite, San Antonio, and Espiritu Santo) is the spread of black mangroves into salt marsh environments that were typically dominated by saltmarsh cordgrass. Marsh environments on bay shorelines (both mainland and back barrier) are an important part of the coastal ecosystem providing hurricane storm surge abatement and erosion control. Saltmarsh cordgrass marshes provide feeding grounds for the endangered whooping cranes because they are a habitat for one of their favorite food source, blue crabs. Salt marshes are also popular among fisherman who come visit the coast (**fig. 74**).

Studies on black mangroves (**fig. 75**) show that the salt tolerant trees might provide improved resistance to sea-level rise and be more resitant to erosion than saltmarsh cordgrass. While the spread of mangroves may appear beneficial at first due to providing

Figure 74. Fisherman in salt marsh at Goose Island State Park

Figure 73. Whooping Crane in Aransas National Wildlife Refuge.

Figure 75. Mangroves on shoreline of a Texas bay.

additional stabilization to the bay shoreline, it is raising concerns because the trees are spreading into habitat that are critical for whooping cranes continued survival. Studies mapping and monitoring the population growth of mangroves on Texas coastal bay shorelines (**fig. 76**) provides vital information to resource agencies pursuing habitat conservation and management for the endangered whooping crane, as well as other coastal resources.

Figure 76 looks at the expansion of mangroves between 2001 and 2013 in the eastern protion of Espiritu Santo Bay (northeast of our current location). Bayucos Island (highlighted by the rectangle)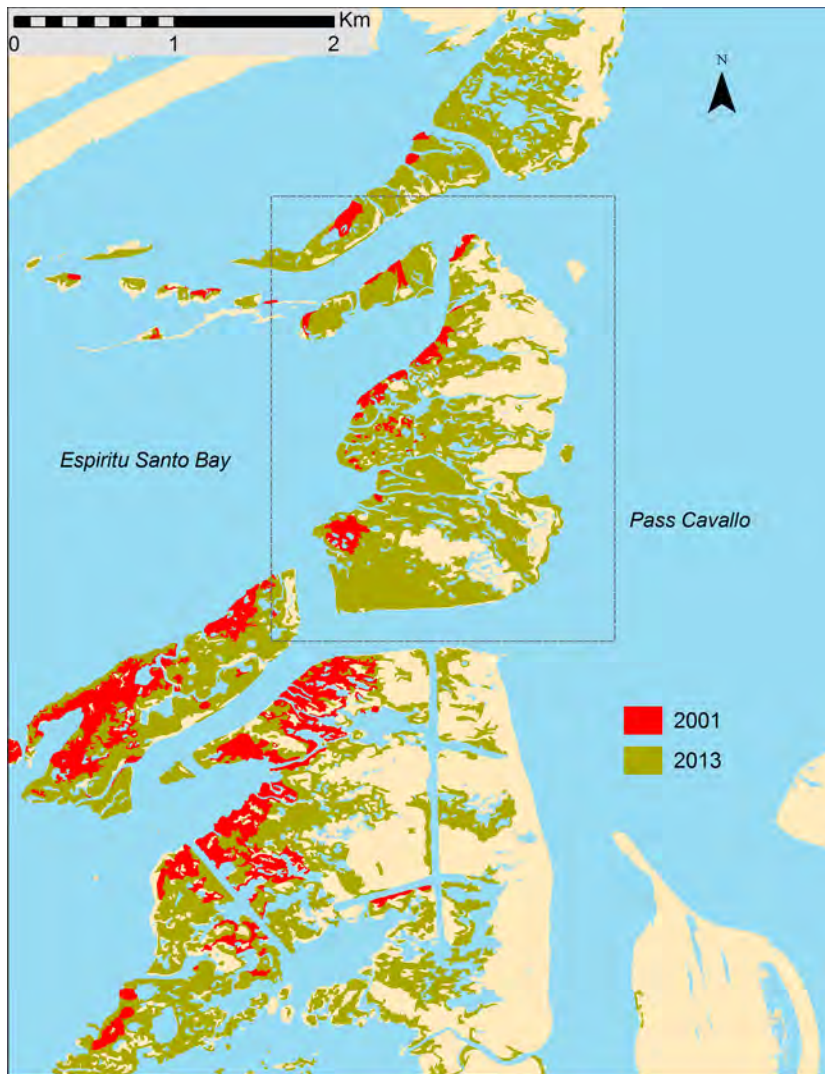 had 124 acres of mangrove in 2001 (red area). By 2013, 983 acres were mapped as having mangrove trees. That is an almost 700% increase in acreage!

Geology: Now let's discuss the underlying geogloy of the area we are standing on. Remember during our lecture last night on the geologic history of Texas bays and estuaries, we discussed that sea level had been flucuating throughout the Pleistocene. During times of extreme cold, sea water was locked in ice sheets and glaciers and sea level was much lower than it is today (lowstand). At other times climate was closer to what we feel today or warmer. The glaciers and ice sheets retreated and sea level rose to levels close to or higher than they are today (highstand). Evidence of the last major highstand was deposited where we are currently standing here at Goose Island State Park. We are standing on the a unit called the Ingleside Sand (part of the Beaumont Formation) that has been interpreted as sediments deposited as a barrier island.

Look at **figure 77**. On San Jose Island and the Gulf facing shores of Aransas and Mequite Bays, modern (Holocene) sediments are being deposited. This geologic unit is quite young, less than 5,000 years old. Now notice that Live Oak Ridge, Lamar Peninsula, and Blackjack Peninsula are all labeled as the same geologic unit. This is Beaumont Formation barrier sand that is Pleistocene aged. Notice the long, linear nature of the formation.

Let's try to imagine how these sediments were deposited. 80,000-120,000 sea level was stabilized at the same level or slightly higher than it is today. Rivers flowing across Texas

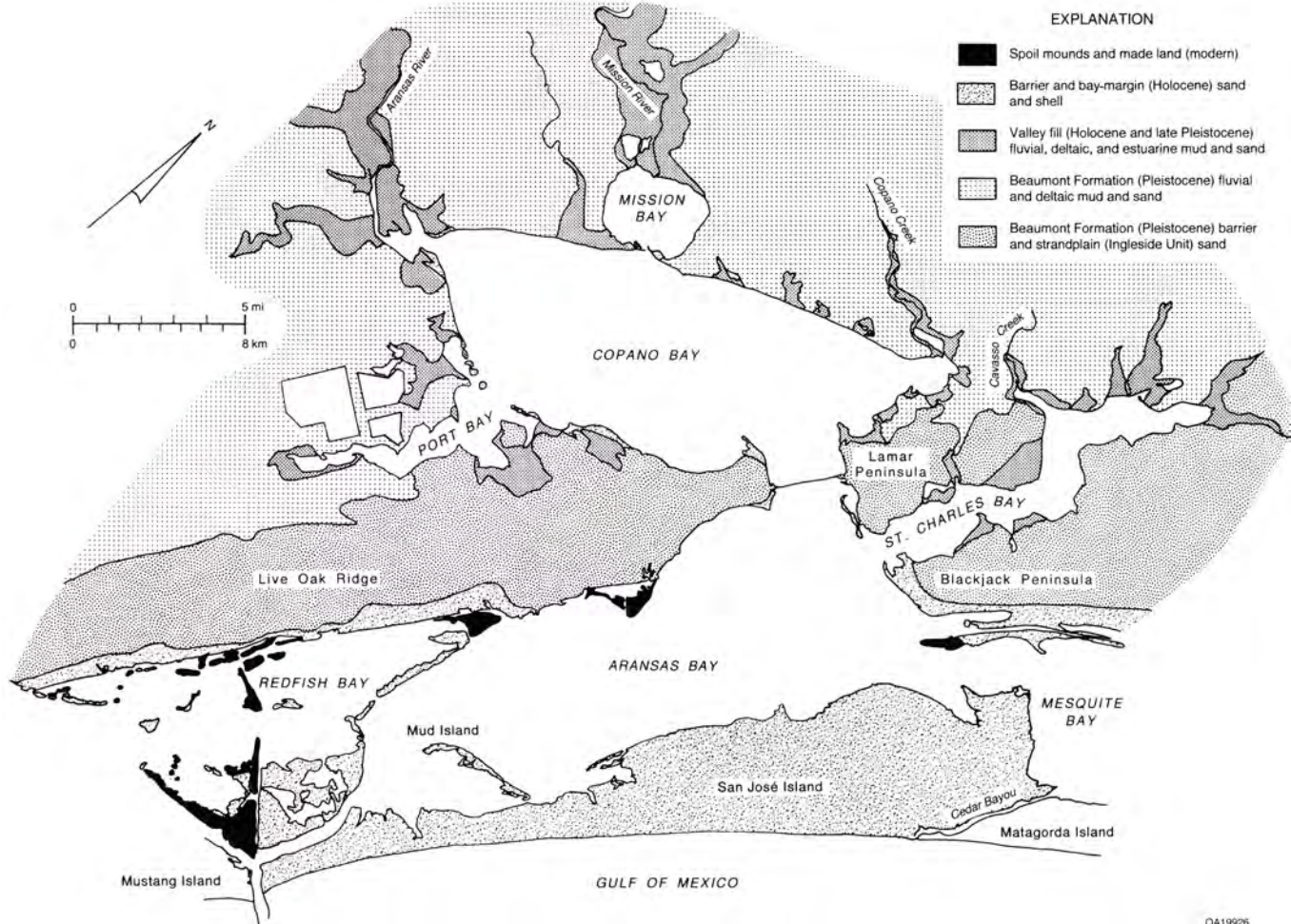Figure 76. Mangrove expansion from 2001 to 2013 in Espiritu Santo Bay.

Figure 77. Generalized geologic map of the Copano and Aransas Bays system. San Jose Island is composed of Holocene age sand and shell. Where we are standing on Pleistocene aged sand (called the Beaumont Formation) from the last highstand.

would have carried sediment and deposited them where the rivers entered the Gulf of Mexico. Waves and currents redistributed the sediments until a small barrier island was born. Through time more and more sand and shells would have been eroded, transported, and deposited by waves, current, wind, and storms (just like we saw on Mustang Island) to create a large barrier island that probably looked very similar to modern day Mustang and San Jose Islands.

Over the next several thousand years, sea level fell stranding the barrier islands sediments. During the last glacial maximum (18,000 years ago) sea level was as much as 400 feet lower than it is today. This was the last sea level lowstand. It marks the end of the Pleistocene

and the start of the Holocene. Sea level began to rise and stabilized near current levels about 5,000 years ago.

Did you know? Relative sea level is rising everywhere along the Texas coast but at different rates. According to the National Oceanic and Atmospheric Administration (NOAA), the tide guage at Rockport has recorded a relative sea level rise of 1.33 feet between 1937 and 2014 (**fig. 78**)! That is a rate of 0.207 inches/year (5.27 mm/yr). At Galveston the rate is higher, 0.25 inches/year (6.34 mm/yr). The Galveston rate might not seem very fast but it means that during the last century sea level has risen over 2 feet!
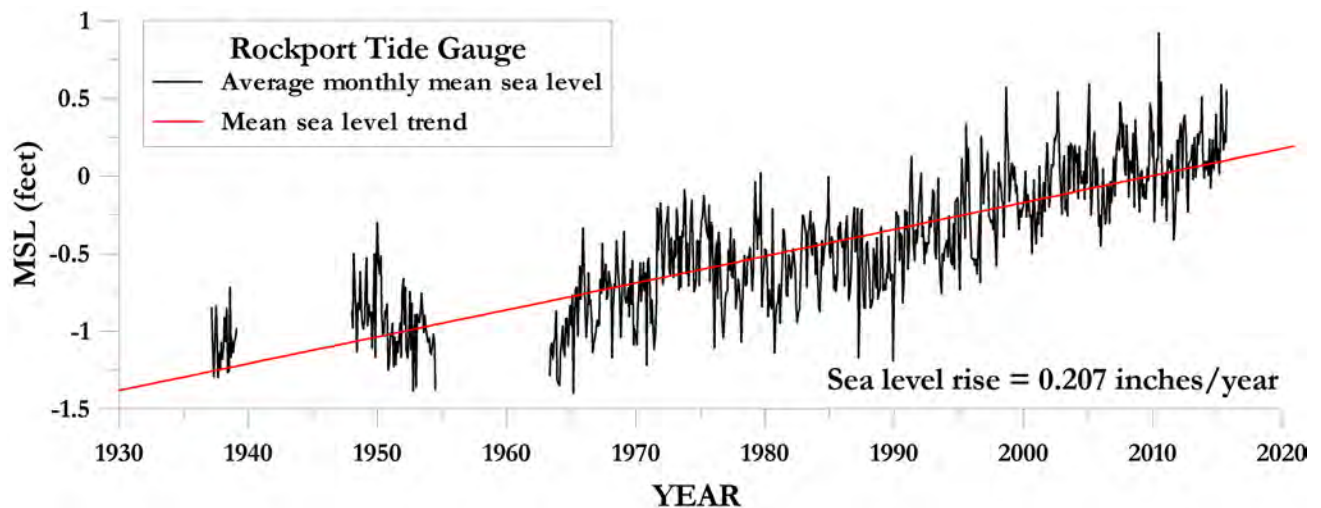
Figure 78. Rockport tide gauge data, 1937-2015 showing sea level rise.

Daily Review

What did we learn today? Today we drove to Port Aransas on Mustang Island. Our only stop was at Goose Island State Park to learn about Aransas and Copano Bays.

Why is what we learned important? Today was your first field stop studying a modern coastal environment. On the shore of Aransas Bay we saw a large estuary and we talked about the importance of this environmnet for wildlife.

Today's geo-words: There were a lot of new terms in last night's lectures. There were no new geo-words added today.

Daily Quiz

Today's **daily quiz** may include questions from the lectures on the Texas coast, bay and estuaries, geologic history, and today's stop.

Tomorrow

Tomorrow we will see how water and wind transport and deposit sediment on a barrier island. On the sunny Texas coast, we spend a lot of time on, in, or near the ocean. Drink plenty of water, wear a hat, and use sunscreen. Have fun, be safe, and learn all you can.

Lectures

We'll spend a few days on the sandy beaches of the Texas coast observing coastal processes. Sand! Sand is a clastic sediment, and we will observe how it is transported and deposited, which means we need to learn about coastal sedimentary processes. After these lectures you should be familiar with the following terms:

- *Barrier island*
- *Beach, dune, barrier flat,* and *lagoon*
- *Forebeach, backbeach, berm,* and *swash zone*
- *Active* and *stabilized dunes*
- *Wavelength* and *wave height*
- *Longshore current* and *longshore drift*
- *Tides*
- *Spring tide* and *neap tide*
- *Tidal range*
- *Washover channel* and *washover fan*
- *Tidal inlet*
- *Flood-tidal delta* and *ebb-tidal delta*